ELSEVIER

Spectrochimica Acta Part B 53 (1998) 1–42

SPECTROCHIMICA ACTA PART B

Review

Fundamental aspects and applications of glow discharge spectrometric techniques

Annemie Bogaerts*, Renaat Gijbels

Department of Chemistry, University of Antwerp, Universiteitsplein 1, B-2610 Wilrijk-Antwerp, Belgium

Received 11 August 1997; revised 24 October 1997; accepted 10 November 1997

Abstract

Glow discharges are kind of plasmas which are used in many fields of application, including analytical spectrometry. This review addresses both the fundamental aspects and analytical applications of glow discharges. In the first part, a systematic overview of the most important plasma processes is presented. To obtain better insight into the complexity of the glow discharge, both mathematical modeling and experimental plasma diagnostics can be carried out. Therefore, the models that were developed for a glow discharge are presented and typical results (e.g. three-dimensional density profiles, fluxes and energy distributions of the various plasma species, the electric field and potential distributions, information about collision processes in the plasma and about sputtering at the cathode, etc.) are summarized. Moreover, the most important plasma diagnostic techniques for glow discharges are discussed. In the second part, an overview is given of the various analytical applications of glow discharges. © 1998 Elsevier Science B.V.

Keywords: Fundamental aspects; Glow discharge spectrometry; Plasma processes

1. Introduction

Glow discharge analytical spectrometric techniques have gained increasing interest in the last few decades, especially in the field of optical emission spectrometry and mass spectrometry. Besides the existing analytical applications which can be found in industrial and service labs (i.e. routine measurements of impurities in metallic alloys or in high-purity metals, depth profiling analyses, e.g. in the automobile industry, etc.), a variety of new developments is being reported in the literature, like the radio-frequency and the pulsed modes, as well as combinations with magnetic fields, microwaves, lasers, etc.

The glow discharge is a kind of plasma which is created by inserting two electrodes in a cell filled with gas at low pressure (e.g. 1 Torr). For analytical applications, argon is most commonly used, but other glow discharges, used for technological purposes, operate more frequently in reactive gases (e.g. N_2, O_2, SiH_4, SF_6, etc.). A potential difference (of the order of 1 kV) is applied between the two electrodes (cathode and anode). This causes 'gas breakdown', i.e. the gas breaks partially up in electrons and positive ions, which results in the formation of the plasma. The positive ions are accelerated towards the cathode by the potential difference and when bombarding they can release secondary electrons and also atoms of the cathode material.

The secondary electrons are accelerated away from the cathode and arrive in the plasma where they can

* Corresponding author. Tel: 0032 3820 2364; Fax: 0032 3 820 2376; e-mail: bogaerts@uia.ua.ac.be.

PII S0584-8547(97)00122-5

give rise to a variety of collisions. The two most important types of collisions are excitation and ionization of gas atoms. The excitation collisions and the subsequent de-excitations to lower levels by radiative decay are responsible for the characteristic 'glow' in the glow discharge (i.e. blue in the case of argon). The ionization collisions create new positive ion–electron pairs; the ions are again accelerated towards the cathode, creating new secondary electrons, which can again give rise to collisions in the plasma, etc. Hence, the combination of ionization collisions in the plasma and secondary electron emission at the cathode makes the glow discharge a self-sustaining plasma.

The atoms of the cathode material, which are released when ions bombard the cathode (this phenomenon is called 'sputtering'), also enter the plasma and can undergo collisions as well. This is the basis of the use of glow discharges for analytical applications. Indeed, the cathode of the glow discharge is constructed out of the material to be analyzed. The analytically important elements are hence sputtered from the cathode and arrive in the plasma. The plasma can therefore be considered as an atom reservoir with a composition characteristic of that of the cathode (i.e. material to be analyzed). The atoms can be probed with an external light source, measuring the resulting absorption or fluorescence. Hence, glow discharges can be used for atomic absorption and fluorescence spectrometry (GD-AAS and GD-AFS). However, the sputtered atoms are also subject to ionization and excitation collisions in the plasma. The ionization collisions create ions of the elements to be analyzed which can be measured in a mass spectrometer, leading to glow discharge mass spectrometry (GDMS). The excitation collisions and the resulting de-excitations give rise to characteristic photons of the elements to be measured; the latter can be detected by an optical emission spectrometer, which results in GD-OES. The latter two techniques, i.e. GDMS and GDOES, comprise most of the applications of glow discharge spectrometry. It should be mentioned that beside applying a direct current (DC) voltage to the electrodes, the glow discharge can also be produced and employed for sputtering purposes with radio-frequency (RF) energy. Indeed, in the latter case, a bias voltage will be built up at one of the electrodes so that net ion bombardment and sputtering can take place.

The above description of the glow discharge is somewhat simplistic. In reality, the glow discharge is a rather complex plasma, existing of a variety of species (i.e. different kinds of atoms, ions, atoms in many excited levels, electrons, photons, etc.) and with a lot of different processes going on. For good analytical practice and for technological applications, a clear understanding of all the processing occurring in the glow discharge plasma is desirable. This can be obtained by plasma diagnostic measurements of the characteristic plasma quantities and by mathematical modeling of the behavior of the various plasma species.

In this review, the basic phenomena going on in the glow discharge plasma will be explained in a systematic way (i.e. the main processes and the dominant plasma species will be discussed) and the state-of-the-art of mathematical modeling and of plasma diagnostic methods will be presented. Since modeling of glow discharges is our major research activity, this topic will be dealt with in somewhat more detail. Furthermore, an overview will be given of the various analytical applications and new developments of glow discharge spectrometry.

2. Fundamental aspects of the glow discharge

2.1. Overview of the basic phenomena

Fig. 1 presents a schematic picture of some of the most important processes and plasma species playing a role in the glow discharge operating in argon. The reality is still much more complicated and probably not all processes are known in the literature. Therefore, it is not feasible to give a complete overview of all possible phenomena. We will therefore restrict ourselves to the most relevant processes in analytical glow discharges, i.e. ionization (and recombination) and excitation (and de-excitation) and to the plasma species playing a role in these processes: electrons, argon atoms, singly charged positive argon ions, argon atoms excited to a variety of energy levels, including the metastable levels, and atoms and ions of the cathode material. Collision processes involving multiply charged particles, clusters and negative ions will not be considered here since these species are assumed to play no dominant role in glow discharge

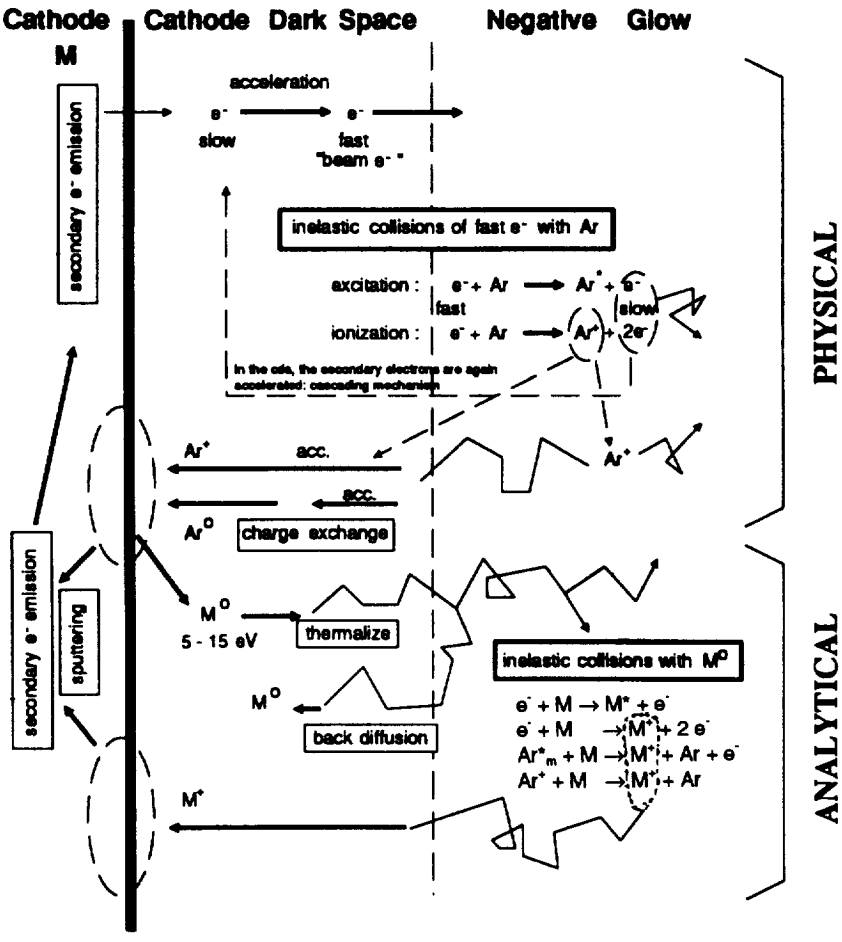

Fig. 1. Schematic representation of some of the main processes occurring in a glow discharge.

and they are not included in our modeling work. In addition to the most important collision processes in the plasma, an overview will be given of the different processes occurring at the walls of the glow discharge cell.

2.1.1. Collision processes in the plasma

2.1.1.1. Elastic collisions. It is worth briefly mentioning this type of collision first because of the high rate at which they occur in the glow discharge. Elastic collisions do not result in internal changes of the energy of the collision partners; their effect is only to redistribute the kinetic energy of the particles. This redistribution is considerable for collisions between species with comparable masses (e.g. two atoms), but is negligible for particles with very different masses (e.g. atom + electron).

2.1.1.2. Ionization and excitation of argon atoms

2.1.1.2.1. Electron impact ionization and excitation

$$Ar^0 + e^- \rightarrow Ar^+ + 2e^-,$$

$$Ar^0 + e^- \rightarrow Ar^* + e^-.$$

Electron impact ionization is one of the most important and best-known processes in the glow discharge. It is the essential process in a self-sustaining plasma since the electrons formed in this way can again give rise to ionization, leading to electron multiplication. It

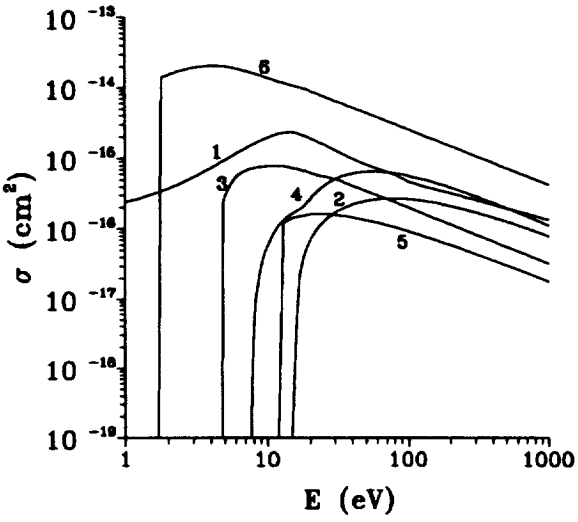

Fig. 2. Illustration of some cross-sections of electron collisions as a function of the electron energies: (1) elastic collisions with Ar atoms; (2) ionization of Ar ground state atoms; (3) ionization of Ar in the metastable levels; (4) ionization of copper atoms; (5) excitation of Ar ground state atoms; and (6) excitation of Ar in the metastable levels.

can occur by the collision of electrons with argon atoms in the ground state (*direct electron impact ionization*) and also with argon atoms in the metastable level at 11.55 or 11.72 eV (*two-step electron impact ionization*). The minimum electron energy required for the first process is 15.76 eV (i.e. the ionization potential of argon), whereas the second process can already occur at electron energies above 4 eV. Nevertheless, the first process is much more important in the analytical glow discharge at voltages of about 1 kV, due to the much higher argon ground-state atom density compared with the argon metastable atom density (see, for example, Ref. [1]). The cross-sections of both processes increase with the electron energy, reach a maximum of about 3×10^{-16} and 8×10^{-16} cm^2 at about 80 and 10 eV, respectively, whereafter they decrease again because the residence time of the electron around the argon atom becomes too short for efficient ionization [2,3] (see Fig. 2).

The mechanism of *electron impact excitation* is the same as for ionization, but less energy is transferred to the atom so that no ionization can occur. Indeed, the electron cannot be ejected, it can only jump to a higher energy level within the atom. The total cross-section of electron impact excitation as a function of the electron energy shows the same behavior as for electron impact ionization. The minimum energy required is 11.55 eV (i.e. the energy of the lowest excited level). A maximum of about 1.6×10^{-16} cm^2 is reached at about 20 eV [4] (see Fig. 2).

2.1.1.2.2. Fast argon ion and argon atom impact ionization and excitation.

$$Ar^0 + Ar_f^+ \rightarrow Ar^+ + Ar_f^+ + e^-, \quad Ar^0 + Ar_f^0 \rightarrow Ar^+ + Ar_f^0 + e^-,$$

$$Ar^0 + Ar_f^+ \rightarrow Ar^* + Ar_f^+, \quad Ar^0 + Ar_f^0 \rightarrow Ar^* + Ar_f^0.$$

In analogy to electron impact ionization and excitation, argon ions and atoms can also cause the ionization and excitation of argon atoms if their energy is sufficiently high. The cross-sections of these processes behave in a similar manner as the ones for electron impact ionization and excitation, i.e. rising with increasing impact energy until a maximum is reached and falling off at high energies [5]. However, the cross-section curves are shifted towards higher energies due to the larger masses of atoms and ions. Indeed, the process becomes only important at ion and atom energies of more than 100 eV and the maximum is reached above 1000 eV (see Fig. 3). The cross-section

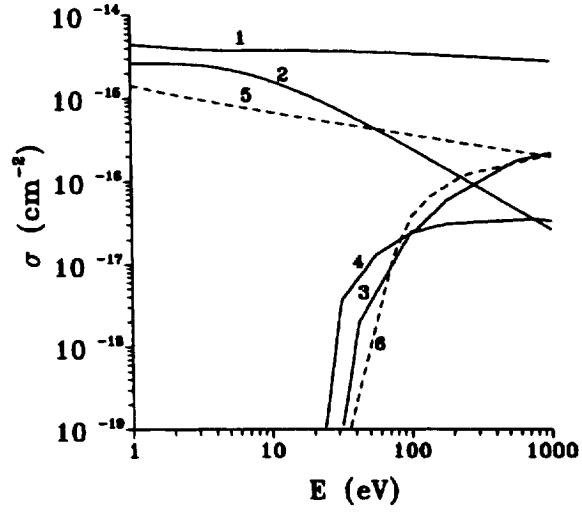

Fig. 3. Illustration of some cross-sections of Ar ion and atom collisions as a function of the ion and atom energies. Solid lines = ion collisions: (1) elastic (isotropic scattering) collisions with Ar atoms; (2) symmetric charge transfer collisions with Ar atoms; (3) ionization of Ar ground state atoms; and (4) excitation of Ar ground state atoms. Dashed lines = atom collisions: (5) elastic collisions with Ar atoms; and (6) ionization and excitation of Ar ground-state atoms.

values at the maximum are comparable with the ones for electron impact excitation and ionization. In the glow discharge, highly energetic argon ions and atoms are only found close to the cathode where they have gained much energy from the electric field in front of the cathode. Therefore, argon ion and atom impact ionization and excitation are only significant close to the cathode and the importance of these processes in the glow discharge increases with increasing discharge voltages. At voltages of about 1 kV which are commonly used in analytical glow discharges, these processes are clearly not negligible (see, for example, [6]).

2.1.1.2.3. Argon metastable atom collisions leading to the ionization of one of the atoms.

$$Ar_m^* + Ar_m^* \rightarrow Ar^+ + Ar^0 + e^-.$$

When two argon metastable atoms collide with each other, they have together sufficient energy (2×11.55 or 11.72 eV) to knock off one electron and to bring about the ionization of one of the atoms. The rate constant of this process is about 6.4×10^{-10} cm^3 s^{-1} [7]. The process is, however, of minor importance in the analytical glow discharge compared with electron impact ionization [1].

2.1.1.2.4. Symmetric charge transfer.

$$Ar_f^+ + Ar_s^0 \rightarrow Ar_f^0 + Ar_s^+.$$

When a fast argon ion collides with a slow argon atom, an electron can be transferred from the atom to the ion without changes in kinetic energy of the two colliding particles. In this way, a fast argon atom and a slow argon ion are formed. It is hence not a real ionization process since there is no increase in the number of ions; only a fast argon ion has disappeared and a new slow argon ion was created. However, the process is included in this overview since it is of major importance in the glow discharge. Indeed, this process is responsible for the creation of a large flux of fast argon atoms bombarding the cathode, which leads to sputtering (see further). The cross-section of this process is at the order of 3×10^{-15} cm^2 at energies of a few electronvolts and decreases slightly towards higher energies [8] (see Fig. 3). It should be mentioned that this process is, actually, a form of elastic collisions because there is no change in kinetic energy of the collision partners [8].

2.1.1.2.5. Thermal ionization/excitation and photo-ionization/photo-excitation. In principle, the argon atoms can be ionized or excited due to any suitable energy input. Therefore thermal and photo-ionization and -excitation are also included in this overview. Thermal ionization/excitation occurs due to the energy received by impact with argon gas atoms or with the atoms of the walls. Since the glow discharge can be considered as a 'cold' plasma (i.e. the gas temperature is about 300 K or slightly higher), the thermal processes can be considered negligible [9]. Photo-ionization and excitation, however, can be of importance [9]. The cross-section of photoionization shows a maximum of about 3.7×10^{-17} cm^2 (i.e. about seven times lower than the maximum in the electron impact ionization cross-section) at the threshold photon energy (i.e. 15.8 eV, corresponding to about 800 Å) and decreases very rapidly towards higher energies. The cross-section of photo-excitation is comparable with the one of photo-ionization [9]. In Ref. [10] it is, however, demonstrated that photo-ionization and -excitation are clearly of minor importance compared with electron (and fast ion and atom) impact ionization and excitation.

2.1.1.3. Ionization and excitation of sputtered (analyte) atoms. In principle, the same processes that cause the ionization and excitation of argon atoms also apply to the ionization and excitation of analyte atoms. However, very little is known of the above mentioned processes concerning the analyte atoms. Only electron impact ionization data [11] and some very limited electron impact excitation data [12] are available from the literature. In addition to the above-mentioned processes, two other collision types seem to be of special importance for the ionization (and possibly simultaneous excitation) of analyte atoms.

2.1.1.3.1. Electron impact ionization and excitation

The mechanisms are the same as for the corresponding processes of argon atoms. The cross-section curve of electron impact ionization as a function of the electron energy is of comparable shape and magnitude for all elements [11]. Therefore, this process can be considered as rather unselective. The electron impact ionization cross-section for copper is presented in Fig. 2. The cross-sections of electron impact excitation of the analyte atoms exhibit similar curves.

2.1.1.3.2. Penning ionization.

$$M^0 + Ar_m^* \rightarrow M^+ + Ar^0 + e^-.$$

If an argon atom excited to one of the two metastable levels collides with an analyte atom, the energy of the metastable level (i.e. 11.55 or 11.72 eV) can be used to ionize the analyte atom if the ionization potential of the latter is lower than the metastable energy. Since most of the atoms of the periodic table have an ionization potential lower than this value, Penning ionization is also more or less unselective. Cross-sections of this process are rather difficult to find in the literature for all elements. However, some empirical formulas are available, expressing a relationship between the cross-section and the mass and radius or polarizability of the colliding particles [13,14]. Generally, the Penning ionization cross-sections between argon metastable atoms and analyte atoms are in the order of 5×10^{-15} cm^2 [13,15]. This process is suggested to be dominant in low pressure discharges [16,17]. Elements which cannot be ionized by Penning ionization in argon include H, N, O, F, Cl and Br.

2.1.1.3.3. Asymmetric charge transfer.

$$M^0 + Ar^+ \rightarrow (M^+)^* + Ar^0.$$

The collision between an analyte atom and an argon ion can lead to the transfer of an electron from the atom to the ion if the energy difference between the argon ion ground state or metastable level and the energy levels of the resulting analyte ion is sufficiently small; the efficiency of this process generally decreases with growing energy difference between the levels. Asymmetric charge transfer is therefore a more or less selective process unlike Penning ionization, which occurs unselectively for all elements having an ionization potential below the argon metastable energy levels independently of the relative position of the levels.

A wide range of cross-section data of asymmetric charge transfer is available in the literature (for an overview, see Ref. [18]). However, most data apply to the high or very high energy range (several tens of electronvolts to megaelectronvolts) and are hence not of interest for the glow discharge where the ions are characterized by thermal energies (especially in the NG which constitutes the major part of the discharge and which is also the most important region for ionization). A number of cross-section data can also be found in the literature for thermal energies (see Ref. [18]), but they mainly concern reactions of rare gases and molecular gases.

Cross-section data of asymmetric charge transfer between rare gas ions and metals are much more difficult to find in the literature. A number of papers have described the asymmetric charge transfer process in a qualitative manner or have shown evidence for the occurrence of this process in glow discharges [19–24]. Quantitative cross-section data, mostly obtained experimentally, are available in the literature, in connection with metal–vapor ion (hollow cathode) lasers, for specific combinations of reactants, for example He^+–Cd [25], He^+–Zn [26], He^+–Hg [27], He^+–Cs [28], He^+–Rb [29], Ne^+–Zn [30], Ar^+–Cu [31] and Xe^+–Ca, Sr [32]. Ref. [32] presents cross-section data for the different combinations of reactions between He^+, Xe^+ or Cs^+ ions with Fe, Mo, Al, Ti, Ta and C atoms at energies ranging from 1 to 5000 eV. To our knowledge, asymmetric charge transfer cross-section data between Ar^+ ions and various transition element metals (Fe, Ta, Mo, etc.) at thermal energies are unfortunately lacking. It is also questionable to deduce the cross-sections from data between other elements. Indeed, the process of asymmetric charge transfer appears to be fairly complicated; for example, it is not always true that the smallest energy difference between energy levels yields the highest cross-section [26].

Because of the virtual nonavailability of the cross-section data, the relative importance of this process in the glow discharge is still a controversial subject. Steers and coworkers have clearly demonstrated the occurrence of asymmetric charge transfer between Ar^+ and Cu, Ne^+ and Cu, Ne^+ and Al, Ar^+ and Fe and between Ar^+ and Ti (see, for example, Refs [20–22]). Recently, Wagatsuma and Hirokawa also showed evidence for the occurrence of this process between Ar^+ and Fe and between Ne^+ and Fe in a Grimm-type glow discharge [23]. The process has also been shown to be important in hollow cathode discharges between Ne^+ and Cu [19,33], Ar^+, Ne^+ and Fe [24], Ar^+ and Ti [34], He^+ and Cu [35] and between Ar^+ and Cu [31]. In the early investigations of Coburn and Kay [16], Penning ionization was considered to be the most important ionization process and charge transfer was neglected. These workers considered only charge transfer in which the ground state of the

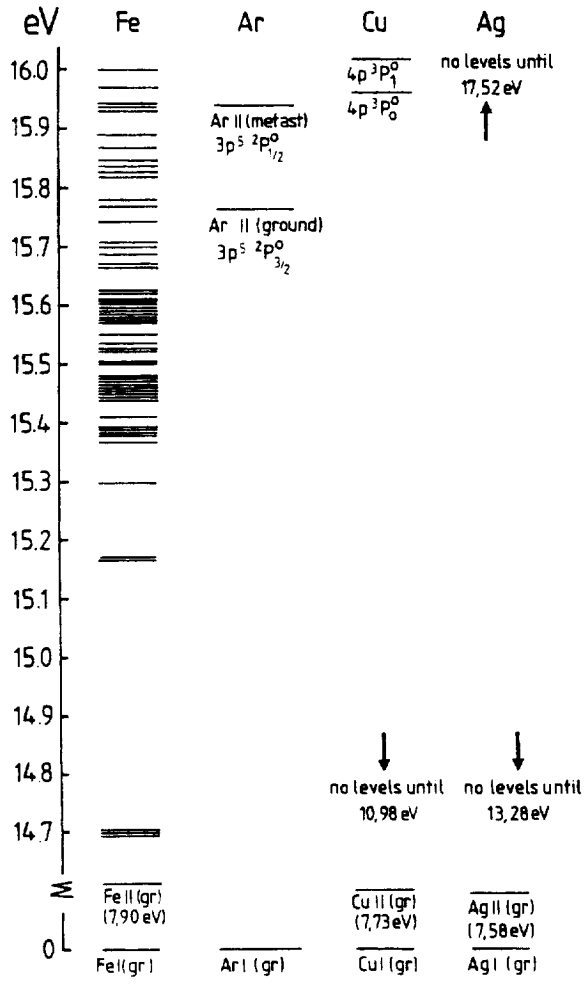

Fig. 4. Schematic representation of the energy levels of the element ions that could account for charge transfer with Ar ions, for three elements (Fe, Cu and Ag). The zero level is taken at the ground state of the atoms. Only the region of interest for asymmetric charge transfer is shown (i.e. 14.7–16.0 eV; the Ar II ground-state and metastable levels are situated at 15.76 and 15.94 eV, respectively, and it is assumed that levels lying from 1 eV below and 0.02 eV above these ArII levels are suitable for asymmetric charge transfer). Reprinted from Ref. [18] with permission of the Royal Society of Chemistry.

analyte ions is formed; since the energy difference is then far too large, they ruled out that possibility. However, as was demonstrated by Steers and coworkers [20–22], the resulting analyte ion can also be formed in an excited state so that the energy difference is much smaller and asymmetric charge transfer becomes, therefore, more probable. In contrast, Levy et al. [17] found that charge transfer between Ar^+ and Cu is unimportant in low-pressure, low-current discharges. Indeed, the Cu ion possesses only one energy level which has a good overlap with the argon ions in the metastable state only (see Fig. 4) and it is probable that the argon ions in the metastable state have low densities in a low-pressure discharge. However, a large number of elements do possess ionic energy levels that have a good overlap with the argon ion ground-state level, but these elements were not investigated in Ref. [17] so that the conclusions of this paper cannot be generalized. In Refs [25,26], cross-section data are available for He^+/Cd and He^+/Zn, respectively; in these cases, a good energy overlap is found and moreover the Penning ionization and asymmetric charge transfer cross-sections are measured to be of comparable magnitude. From the argon ion number densities that we have calculated (see, for example, Refs [36,37]), we expect that asymmetric charge transfer can have a non-negligible role for specific elements, also in low pressure glow discharges (see, for example, Refs [1,38,39]).

The energy levels of argon ions and of ions for three elements (Fe, Cu and Ag) are shown schematically in Fig. 4 to illustrate for which elements asymmetric charge transfer with argon is possible [18]. It can be seen that FeII possesses many levels suitable for asymmetric charge transfer; CuII has no levels lying close to the ArII ground state and only one level showing close overlap with the ArII metastable state; AgII has no levels at all that could account for asymmetric charge transfer with argon.

2.1.1.4. Positive ion–electron recombination. Electron–ion recombination is the reverse process of ionization, i.e. an electron coalesces with a positive ion to form a neutral atom. From the conservation laws of momentum and energy follows that a simple two-body coalescence is not allowed [9]. However, some alternative recombination processes can occur. To our knowledge, the recombination processes apply to both argon and analyte ions and they will therefore be discussed simultaneously (A^+ is an arbitrary ion).

2.1.1.4.1. Three-body recombination.

$$A^+ + e^- + B \rightarrow A^0 + B.$$

A third body takes part in the collision process, taking

away the excess energy and allowing the conservation laws to be satisfied. The third body B can be every particle present in the plasma, or it can be the cell wall. If the third body is a heavy particle, the electron can lose only a small fraction (i.e. $2m_e/M_B$) of its energy to the third body. Therefore, this reaction is very slow [40]. Massey and Burhop [41] estimated that the coefficient of this three-body recombination process is about $10^{-11} \times p$ cm^3 s^{-1}, where p is the gas pressure in Torr. Therefore, for a gas pressure of about 1 Torr and for electron and argon ion densities in the order of 10^{11} cm^{-3} [36,37], the rate of this recombination process is of the order of 10^{11} cm^{-3} s^{-1}. When comparing this with typical ionization rates in the order of 10^{16} cm^{-3} s^{-1} (see Refs [6,36,37]), it can be concluded that this kind of recombination is insignificant for the typical analytical glow discharge conditions. However, when the third body is an electron, the three-body recombination process is clearly more efficient since the electrons can better take away the excess energy. Rate constants for this process are reported in the order of 10^{-24} cm^6 s^{-1} [42]. For electron and argon ion densities in the order of 10^{11} cm^{-3}, the rate of this recombination is about 10^9 cm^{-3} s^{-1}. Hence, this process is also negligible compared with ionization in the analytical glow discharge.

2.1.1.4.2. Radiative recombination.

$$A^+ + e^- \rightarrow A^* + h\nu.$$

The excess energy is carried away by a photon. The rate constant of this process is about 10^{-11} cm^3 s^{-1} in the case of argon [43], yielding a recombination rate of about 10^{11} cm^{-3} s^{-1} at typical electron and argon ion densities, which is again negligible compared with the ionization rate.

2.1.1.4.3. Dissociative recombination.

$$AB^+ + e^- \rightarrow (AB)^* \rightarrow A^* + B.$$

When the ion is molecular, a two-body recombination process is possible since the collision product can dissociate and the recombination energy is converted into kinetic and potential energy of the dissociation products. When AB^+ is equal to Ar_2^+, the rate constant is in the range of 10^{-7}–10^{-6} cm^3 s^{-1} [43]. The process is hence clearly more efficient than radiative recombination. Nevertheless, this process will not be of major importance in the glow discharge since Ar_2^+ ions are not considered to be dominant species in the glow discharge plasma.

2.1.1.4.4. Two-stage recombination.

$$A^0 + e^- \rightarrow A^-,$$

$$A^- + A^+ \rightarrow A^0 + A^0.$$

The electron attaches to a neutral atom to form a negative ion. The negative ion collides with a positive ion, an electron is transferred and two neutral atoms are formed. The probability of forming a negative ion (step 1) depends on the electronegativity of the atom. For argon, this probability is very low so that this kind of recombination is also negligible in an argon discharge.

In general, it can be concluded that electron–ion recombination is only significant at high electron and ion densities and will be of minor importance in the low-pressure analytical argon glow discharges discussed in this review.

2.1.1.5. De-excitation. As recombination is the inverse of ionization, de-excitation is the inverse of excitation. Indeed, except from the metastable levels, the excited levels of the atoms are only short-lived and the electron configuration soon returns to the ground state in one or several transitions. Each transition is accompanied by the emission of a photon with specific energy. If such a photon has an energy between 1.7 and 3.0 eV (corresponding to 720 and 410 nm, respectively), it is detected by the human eye. Hence, the de-excitation processes produce a glow and are therefore responsible for the characteristic name of the 'glow' discharge.

2.1.2. Processes occurring at the walls

When a particle collides at the walls of the glow discharge cell, different phenomena may occur depending on the kind of particle. An electron may be reflected, absorbed or cause the emission of secondary electrons. An ion or atom may be reflected (possibly in another form), implanted (probably with structural rearrangements), cause secondary electron emission or eject one of the wall atoms (called sputtering). The latter two processes are of special importance for the analytical glow discharge and will therefore be discussed in more detail. Secondary electron emission can occur at all walls, whereas

sputtering is more or less restricted to the cathode since high particle bombarding energies are required for this process.

2.1.2.1. Secondary electron emission. When a particle strikes a surface, an electron can be emitted. This process is necessary to maintain the glow discharge, i.e. new electrons can be supplied to compensate for the electron losses at the walls. Secondary electron emission can be caused by the bombardment of electrons, ions, neutrals and photons. The number of electrons emitted per incident particle is called the secondary electron emission coefficient. It depends on the kind of bombarding particles and their energy and on the kind of wall material.

2.1.2.1.1. By electron bombardment. This process is only important at the anode walls and is negligible at the cathode since the strong electric field in front of it prevents the electrons from bombarding the cathode. When electrons strike a surface, three types of electrons are emitted (see Fig. 5, [9]), i.e.: (1) the elastically reflected primaries with energies equal to the energy of the incident electron; (2) inelastically reflected primaries, with energies lower than the incident electron energy; and (3) true secondary electrons, with energies of a few electronvolts. The latter group is often the major one. The secondary electron emission coefficient by electron bombardment, δ, is in the order of 1, but depends on the electron energy and the kind of surface material. It typically shows a maximum at electron energies of about 600–800 eV [9].

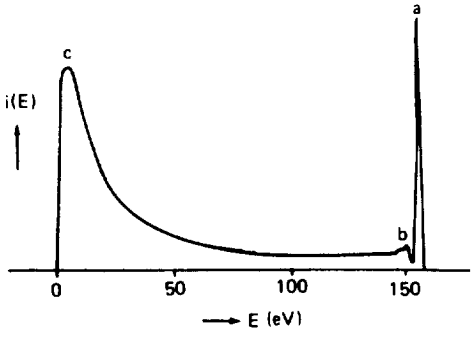

Fig. 5. Energy distribution of secondary electrons emitted due to electron bombardment on a silver surface: (a) elastically reflected primaries; (b) inelastically reflected primaries; (c) true secondary electrons. Reprinted from Ref. [9] with permission of John Wiley and Sons, Inc.

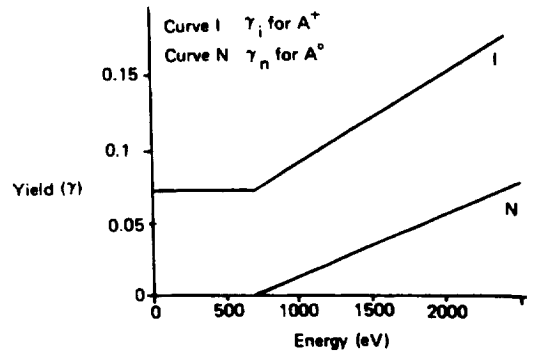

Fig. 6. Secondary electron emission coefficient for Ar ion and atom bombardment of a Mo surface, as a function of the ion and atom energies. Reprinted from Ref. [9] with permission of John Wiley and Sons, Inc.

2.1.2.1.2. By atom and positive ion bombardment. This process can occur at both cathode and anode walls. For clean surfaces, the secondary electron emission coefficient, γ, is nearly independent of the ion or atom kinetic energy at energies below 500–1000 eV. It is typically in the order of 0.1 for positive argon ions and nearly zero for neutral ground-state argon atoms. At higher energies, γ starts to increase with the ion or atom kinetic energy (see Fig. 6, [9]). This suggests that secondary electron emission results from a constant potential energy component (approximately 0.1 for the argon ions and almost zero for the argon atoms) and a kinetic energy component (equal for both) which only plays a role at energies beyond 500–1000 eV. The mechanism of 'potential energy ejection' is explained by Auger neutralization. The potential energy component of the ions is of the order of the ionization potential, which seems amply sufficient for secondary electron emission. Neutral ground-state atoms do not possess such a potential energy component which explains that γ is negligible at energies below 500–1000 eV. However, metastable atoms do possess a potential energy (i.e. the energy of the excited metastable level); hence, they will give rise to a higher secondary electron emission coefficient. However, rather little quantitative information is available. For helium (2^3S) metastables, a secondary electron emission coefficient of 0.29 on a gold surface was reported by Stebbings [44]. Hasted

extended this work and observed values in the order of 0.1–0.25 for surfaces of molybdenum, tungsten and platinum [45]. Oechsner measured secondary electron emission coefficients for 1.05 keV Ar^+ ions on 11 different polycrystalline surfaces [46]. He proposed a theoretical formula which showed good agreement with the experimentally obtained values:

$$\gamma = \frac{0.2}{\varepsilon_F}(0.8E_i - 2\Phi),$$

where ε_F is the Fermi energy measured from the bottom of the valence band, E_i is the effective potential energy of the incoming ion and Φ is the work function of the metal. If this formula is applicable to other species than Ar^+ ions too, the secondary electron emission coefficient of argon metastable atoms ($E_i = 11.55$ or 11.72 eV) on metal surfaces can be calculated and typical values of about 0.005–0.05 would be obtained.

It should be noted that the value of the secondary electron emission coefficient by ion and atom bombardment is largely dependent on the surface conditions (crystal phase, contaminations). Indeed, it appears that for contaminated surfaces, the secondary electron emission coefficients of both argon ions and atoms can vary over many orders of magnitude as a function of the bombarding energies [47]. Moreover, the values characteristic for pure metals can differ significantly from the ones of alloys or nonconducting materials [9].

2.1.2.1.3. By photon bombardment. The ejection of electrons due to photon bombardment is called photo-emission. The photoelectric yield γ_p for most pure metals is only 10^{-3} electrons per photon in the visible and near uv wavelength range since the photons are usually more efficiently reflected. It increases, however, towards shorter wavelengths (i.e. of the order of 0.1 at 100 nm [9]). The effects of photoelectric emission in glow discharges are, however, not well understood.

2.1.2.1.4. Field emission. At extremely high electric fields (approximately 10^7 V/cm), electrons can be emitted by the mere action of the electric field. However, since such high electric fields do not occur in analytical glow discharges, this effect can be considered negligible.

2.1.2.2. Sputtering. When energetic particles (i.e. gas ions, gas atoms and also ions of the cathode material) bombard the cathode surface, they can penetrate into the surface and set up a series of collisions between atoms of the cathode material, until they have lost their energy. In this three-dimensional collision cascade which lasts for a very short period of time only (approximately 10^{-12} s [48]), atoms lying at the surface can obtain some energy larger than their surface binding energy so that they can escape from the surface. This is called sputtering. It is believed that the majority of the sputtered particles are neutral atoms. Ions can also be sputtered, but positive ions will immediately return back to the cathode, by the strong electric field in front of it. The energy of the sputtered atoms is in the order of 5–15 eV [49].

An important quantity with respect to sputtering is the sputtering yield, Y. It is defined as the number of sputtered atoms per incident particle. Analytical expressions or estimates for sputtering yield data were developed by many authors from theories [50], empirical relationships [51,52] and computer simulations [53] of sputtering processes. Sigmund has developed a comprehensive theory describing the effects of different ion–target combinations and energies, based on the assumption that sputtering is closely related to other ion-bombardment phenomena and solving the linearized Boltzmann equation [50]. The calculation consists of four different steps: (1) the determination of the amount of energy deposited by energetic particles near the surface; (2) the conversion of this energy into a number of low energy recoil atoms; (3) the determination of the number of these atoms that can reach the surface; and (4) the selection of those atoms that have sufficient energy to overcome the surface binding forces. However, systematic derivations from the original Sigmund formula were pointed out for some cases, such as light-ion and low-energy sputtering [51]. A few modifications to this original formula were proposed, but some discrepancies still remained. However, a number of empirical formulas were also developed [51,52] in which the discrepancies of the Sigmund formula were solved and which can hence be applied to all ion–target combinations [52]. In our modeling calculations, we use the so-called second Matsunami formula for normal incidence [51,52]:

$$Y(E) = 0.42\frac{\alpha Q K \sigma_n(\varepsilon)}{U_s[1 + 0.35U_s\sigma_e(\varepsilon)]}\left[1 - \sqrt{\frac{E_{th}}{E}}\right]^{2.8},$$

where $Y(E)$ is the sputtering yield for incident ions (and atoms) of energy E; U_s is the sublimation energy of the cathode material (in eV); Q is an empirical parameter, dependent on the cathode material; and $\sigma_e(\varepsilon)$ and $\sigma_n(\varepsilon)$ are Lindhard's elastic and inelastic reduced stopping cross-sections

$$\sigma_e(\varepsilon)=0.079\frac{(M_1+M_2)^{3/2}}{M_1^{3/2}M_2^{1/2}}\frac{Z_1^{2/3}Z_2^{1/2}}{(Z_1^{2/3}+Z_2^{2/3})^{3/4}}\sqrt{\varepsilon},$$

$$\sigma_n(\varepsilon)=\frac{3.441\sqrt{\varepsilon}\ln(\varepsilon+2.718)}{1+6.355\sqrt{\varepsilon}+\varepsilon(-1.708+6.882\sqrt{\varepsilon})},$$

in which ε is the reduced energy,

$$\varepsilon=\frac{0.03255}{Z_1Z_2(Z_1^{2/3}+Z_2^{2/3})^{1/2}}\frac{M_2}{M_1+M_2}E,$$

where Z_1 and Z_2 are the atomic numbers of the bombarding and sputtered particles, respectively, and M_1 and M_2 are their mass numbers.

K is the conversion factor from $\sigma_n(\varepsilon)$ to $S_n(E)$ (reduced energy to energy in eV):

$$K=\frac{S_n(E)}{\sigma_n(\varepsilon)}=8.478\frac{Z_1Z_2}{Z_1^{2/3}+Z_2^{2/3})^{1/2}}\frac{M_1}{M_1+M_2}.$$

α is an empirical parameter, a function of M_1/M_2:

$$\alpha=0.08+0.164\left(\frac{M_2}{M_1}\right)^{0.4}+0.0145\left(\frac{M_2}{M_1}\right)^{1.29}.$$

E_{th} is an empirical parameter, a function of M_1/M_2 and U_s. It represents the threshold energy required for sputtering:

$$E_{th}=U_s\left[1.9+3.8\left(\frac{M_1}{M_2}\right)+0.134\left(\frac{M_2}{M_1}\right)^{1.24}\right].$$

This empirical formula is, in principle, valid for all combinations of bombarding ions/atoms and cathode materials [52].

From this formula, it can be concluded that the sputtering yield is a complex function of the incident energy and the masses and atomic numbers of the bombarding particles and surface target. The influence of the different factors determining the sputtering yield will be briefly discussed.

2.1.2.2.1. The kind of discharge gas. Inert gases are mainly used since they provide high sputtering yields and they will not undergo chemical reactions with the cathode material.

2.1.2.2.2. The masses of the incident particles. In general, the sputtering yield increases less than linearly with the masses of the bombarding particles. H_2^+ forms an exception, i.e. it gives unusually high sputtering yields due to chemical reactions with the cathode material which result in low redeposition. From the Matsunami formula (see above), it can also be concluded that the sputtering yield does not reach a maximum when the masses of bombarding particles and surface target are close to each other (see examples in Ref. [52]), which has sometimes been suggested from simplified sputtering yield expressions.

2.1.2.2.3. The energy of the incident particles. A threshold energy of the incident particles is required to give sputtering. Indeed, the atoms at the cathode surface must obtain sufficient energy to overcome their surface binding energy. A good measure of the surface binding energy is the heat of sublimation. It is suggested that the minimum energy for sputtering must be about four times the heat of sublimation of the cathode material [48]. Above this minimum energy, the sputtering yield increases with the energy of the bombarding particles. It reaches a broad maximum at energies in the order of several kiloelectronvolts, whereafter it decreases again, as ion implantation becomes important [9].

2.1.2.2.4. The angle of the incident particles. Oechsner has found that for rare gas ions bombarding a polycrystalline copper target with energies of 0.5–2 keV, the sputtering yield reaches a maximum at incident angles of about 60°–80° relative to the surface normal [54]. Indeed, at low incident angles, the sputtering yield increases with rising angle due to the increased probability of the collisional cascade to propagate back to the cathode surface and hence to result in sputtering. At incident angles higher than 60°–80°, the sputtering yield decreases since the incoming particles are more likely to reflect off the surface without any penetration or momentum transfer so that sputtering becomes unlikely.

It should be mentioned that these sputter angle studies were performed with ion guns in a vacuum setting where perfect control of the sputtering angles is possible. This is, however, not the situation in a glow discharge. It is expected that the majority of the ions from the glow discharge plasma bombard

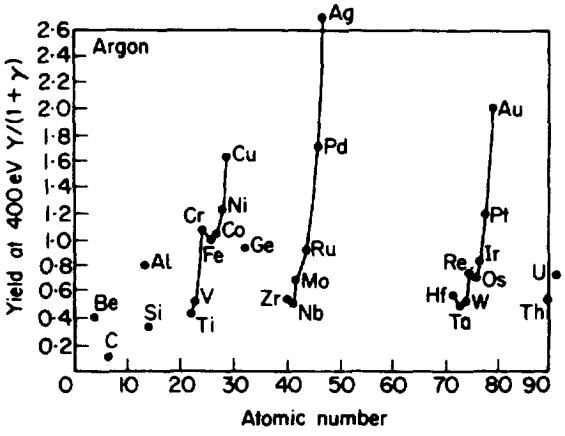

Fig. 7. Sputtering yields of various transition elements due to bombardment of Ar ions with energy of 400 eV. Reprinted from Ref. [55] with permission of John Wiley and Sons, Inc.

the cathode in a perpendicular direction because they are directed by the electric field in front of the cathode. However, the argon atoms are subject to a large number of scattering collisions and can in principle bombard the cathode from all directions. Since the latter species play a dominant role in the sputtering process [38], the results of the above mentioned sputter angle studies are not directly applicable to glow discharge sputtering.

2.1.2.2.5. The kind of cathode material. In general, the sputtering yield increases with the atomic number of the cathode material, within each row of the periodic table (see Fig. 7, [55]). Copper, silver and gold have the highest sputtering yield among transition metals. This trend is explained in the following manner [56]: it is stated that if the penetration depth in the surface increases, a larger fraction of the energy is expended in collisions that do not lead to sputtering. The increase in sputtering yield is associated with the filling of the electron shells, especially the d shells. As the shells fill, the target looks more opaque and the incident particles are not able to penetrate very deeply and give hence rise to more sputtering.

However, it should be noted that the sputtering yields of the different elements seldom differ more than a factor of ten among each other, as opposed by the rates of evaporation which differ by several orders of magnitude [48]. Owing to these rather uniform sputtering yields, the glow discharge is relatively free from matrix effects.

2.1.2.2.6. The cathode surface. Besides the kind of cathode material, also the cathode surface has influence on the sputtering yield, i.e. the sputtering yield decreases by surface contaminations, or by the formation of oxide layers or adsorbed gas layers on the cathode surface. Moreover, the sputtering can result in the formation of a regular pattern of submicroscopic cones on the surface. These are due to some components in the cathode material with a lower sputtering yield. These components can migrate over the cathode surface and form small clusters, thereby protecting the underlying material from sputtering. This effect also results in a decrease of the sputtering yield.

2.1.2.2.7. The cathode temperature. At typical glow discharge conditions the sputtering yields decrease slightly with increasing temperature since the more loosely bound atoms on the surface tend to be annealed to positions of stronger binding [48].

2.2. Spatial zones in the glow discharge

The glow discharge can be subdivided into various regions between cathode and anode, differing in radiation intensity, potential and electric field distribution, space charge and current density (see Fig. 8, [9]). The actual position and the occurrence of the various regions depend on the discharge parameters, like pressure, voltage, current, kind of gas and distance between cathode and anode. In this section, a short description of the different regions will be given and the influence of the parameters will be explained. The description is made for large discharge cells, where all regions are present. It has to be mentioned that the glow discharge used for analytical purposes is relatively small and does in general not contain all the regions.

2.2.1. The cathode dark space

The cathode dark space (CDS) is the thin, dark layer in front of the cathode, also called 'Crookes' or 'Hittorf' dark space. Strictly speaking, it is not completely dark, but appears so to the eye in comparison with the other more luminous parts of the discharge. It includes actually a number of dark and bright layers. The *electrical current*

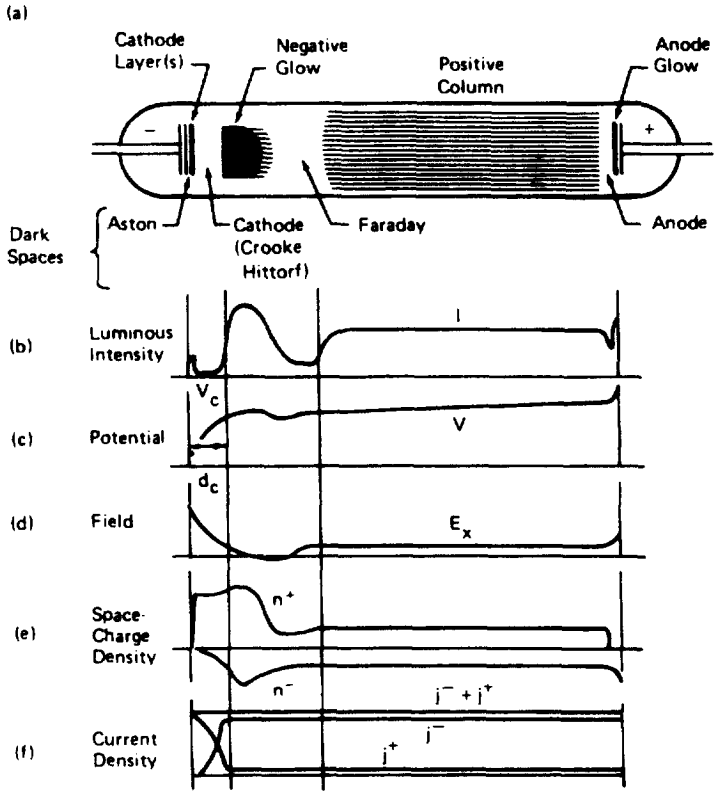

Fig. 8. Schematic representation of the subdivision of the glow discharge into different regions (a); differing in luminous intensity (b); potential distribution (c); electric field (d); space charge density (e); and current density (f). Reprinted from Ref. [9] with permission of John Wiley and Sons, Inc.

in this region is mainly carried by the gas (argon) ions.

The cathode dark space is the *most important part* of the discharge. It is the essential zone to sustain the discharge. Electrons leave the cathode and are accelerated by the electric field in front of the cathode. When they have acquired sufficient energy, they can cause ionization collisions, thereby creating new electrons (electron multiplication) and also ions. The ions are accelerated towards the cathode. Upon bombardment on the cathode, they release new electrons which can again produce ionization collisions. In this way, the continuity of the processes is ensured and the glow discharge is self-sustaining.

The cathode dark space is characterized by a *large potential difference*. Almost the entire potential difference between anode and cathode falls off in the cathode dark space; therefore, it is also called cathode fall, V_c. The large potential difference over a small distance gives rise to a high electric field in the cathode dark space. The electric field is extremely negative at the cathode and goes more or less linearly to virtually zero at the end of the cathode dark space.

Due to the high cathode fall, the electrons will be accelerated to high velocities and they will not play a significant role in determining the space charge. The ions will not reach such high velocities due to their much higher masses (lower mobilities) and therefore they will determine the space charge. Hence, the cathode dark space is characterized by a *highly positive space charge*. The latter is, in turn, responsible for the characteristic potential and electric field distributions via Poisson's equation.

The *optical characteristics* of the cathode dark space are determined by the occurrence of excitation processes of the plasma species (electrons, ions, fast

atoms). If the species possess the amount of energy for efficient excitation (approximately 20 eV for electrons, higher than 100 eV for the ions and atoms), they will cause excitation collisions and the subsequent de-excitations are responsible for the emission of radiation. The electrons leave the cathode with energies of a few eV. This is too low for excitation, resulting in a very thin dark layer at the cathode (the Aston dark space). They attain, however, rapidly the energy suitable for excitation, giving rise to a small bright layer (the first cathode layer). These two thin layers can in principle be sharply distinguished since the electrons still have beam characteristics close to the cathode, i.e. all electrons have nearly the same energy and reach hence at the same place the maximum probability for excitation. After the excitation collisions in the first cathode layer, the electrons have lost their energy and they possess, again, not enough energy for excitation; hence, a dark layer arises. When the electrons have once more received sufficient energy for excitation, the second cathode layer is formed. Since some electrons have undergone collisions, whereas others have not, and since secondary electrons are created in ionization collisions, the electron beam is not monoenergetic anymore. Therefore, the second cathode layer is rather vague and a third cathode layer is probably not visible anymore. On their further trajectory away from the cathode, the electrons gain much energy from the electric field and their energy becomes too high for efficient excitation (see Fig. 2 for the excitation cross-section as a function of the electron energy). Therefore, the remaining part of the cathode dark space is rather dark. Beside the electrons, the gas (argon) ions and fast atoms can also give rise to excitation. The latter processes occur only at sufficiently high ion and atom energies (100–1000 eV and more) and are therefore only significant at high discharge voltages and sufficiently close to the cathode. These processes give rise to a bright layer at the cathode, *the cathode glow*. Moreover, if the cathode is covered with a thin metallic or oxide layer of an alkali or alkaline earth (MgO, Na_2O, Li_2O), another kind of bright layer is present at the cathode, *the cathode light*. This arises from the strongest spectral lines of these elements when they are sputtered away from the cathode.

The *energy distribution* of electrons and ions in the cathode dark space depends on the pressure and voltage in the cell. At low pressure and high voltage, the collision frequency of electrons and ions is rather low and they will therefore be more or less monoenergetic with energies approaching the total discharge voltage. At higher pressure, there will be more collisions and the energy will be spread out, giving rise to a certain energy distribution. The energy distribution of the various charged plasma species is clearly not Maxwellian since the particles gain more energy from the electric field than they lose by collisions. Therefore, it is stated that the cathode dark space is far from hydrodynamic thermal equilibrium.

2.2.2. The negative glow

The negative glow (NG) is the bright, large region adjacent to the cathode dark space. It is more or less *equipotential* and *field-free*. The electrons are hence not accelerated any more, but are slowed down by collisions. Therefore, they will play a role, together with the argon ions, in determining the space charge. Positive and negative space charges are more or less equal to each other, resulting in *charge neutrality*. The *electrical current* is predominantly carried by the electrons.

The *optical characteristics* of the negative glow are explained by the fact that the electrons do not gain energy any more, but lose their energy in various collisions. Since the number of electrons in this region is much higher (due to electron multiplication) and since they possess more suitable energies for excitation, the number of excitation collisions is much higher. Therefore the negative glow is characterized by a bright light, the color of which depends on the discharge gas [57]. In the case of an argon discharge, the negative glow possesses a blue color [57]. When the electrons travel through the negative glow, they lose their energy. At the end, they have too low energies for excitation, resulting in a much lower light intensity. The maximum light intensity is therefore observed in the beginning and center of the negative glow.

The *energy distribution* of electrons in the negative glow is more spread out towards lower energies. When the negative glow is sufficiently long, the electrons will be more or less thermalized (Maxwellian distribution) at the end of this region. However, in the negative glow of a glow discharge cell used as ion source for mass spectrometry which is usually rather

small (a few centimeters), electrons with energies ranging from thermalized to the total discharge voltage (primary electrons) can still be present (see, for example, Ref. [36]).

2.2.3. The Faraday dark space

The Faraday dark space is not always present in analytical discharges. It is a dark and *nearly equipotential* region. Due to the large electron multiplication in the negative glow, a small excess of electrons is found at the end of the negative glow. This *net negative space charge* leads to a *small negative electric field* in the Faraday dark space, which draws the electrons out of the negative glow into the Faraday dark space. The *electrical current* in this region is therefore carried by the electrons.

Concerning the *optical characteristics*, the Faraday dark space can be considered as a repetition of the Aston dark space: the electrons leave the negative glow with too low energies for excitation. Therefore, the Faraday dark space is rather dark. However, in rare gas discharges, the Faraday dark space is sometimes characterized by a halo of light. This phenomenon is explained by the radiation emission of metastable atoms in collisions with ground-state atoms.

2.2.4. The positive column

The positive column is again a rather luminous region, but not as bright as the negative glow. It is only present in the discharge at sufficiently large cathode–anode distances, which is mostly not the case in analytical discharges. This region is also *nearly equipotential*. It is characterized by *charge neutrality* and a *small negative constant electric field*. The *current* is carried by electrons which are accelerated by the electric field.

The *optical characteristics* of the positive column can be explained as follows. The electrons will again gain energy by the electric field. The interface between Faraday dark space and positive column is defined as the position where the electrons have enough energy for excitation and ionization. Therefore, the positive column is a bright zone. The interface between Faraday dark space and positive column is, however, rather unsharp since the electrons are not monoenergetic, but can have widely different energies, reaching the optimum energy for excitation at different positions. The color of the positive column is also characteristic for the discharge gas, but differs from the color in the negative glow and is less intense. The positive column of an argon discharge is characterized by a dark red color [57].

The positive column can have a uniform outlook or can be filled with *striations*, i.e. bright and dark layers which can be stationary or moving. The occurrence of striations is explained in the same way as the cathode layers in the cathode dark space, i.e. the electrons gain energy from the electric field, cause excitation (bright layer), lose thereby energy so that they cannot give rise to excitation any more (dark layer), gain once more energy, etc.

The formation of the positive column with the increase of cathode–anode distance is explained in the following way. The electrical current in the Faraday dark space is carried by electrons which leave the negative glow and travel towards the anode. When the distance between cathode and anode increases some of these electrons are lost due to diffusion towards the walls. To compensate for this loss and to produce sufficient electrons that ensure the electrical current towards the anode, the positive column is formed and its small negative electric field directs the electrons towards the anode.

It is stated that the positive column approaches the characteristics of a plasma in hydrodynamic thermal equilibrium since the *energy distribution* of the electrons in this region is more or less Maxwellian.

2.2.5. The anode zone

The characteristics of this region differ according to whether the anode is in contact with the positive column, the Faraday dark space or the negative glow.

When the anode is in touch with the positive column, a negative electric field and a potential increase are required in front of the anode to attract electrons and to guarantee the electrical current to the anode (see above). When the distance between cathode and anode decreases, the positive column disappears and the anode will be in direct contact with the Faraday dark space. Since the latter region is characterized by an excess of electrons, a potential increase is not required to ensure the electrical current to the anode. Hence, the anode is at equipotential with the bulk plasma and there is no electric field in front of the anode.

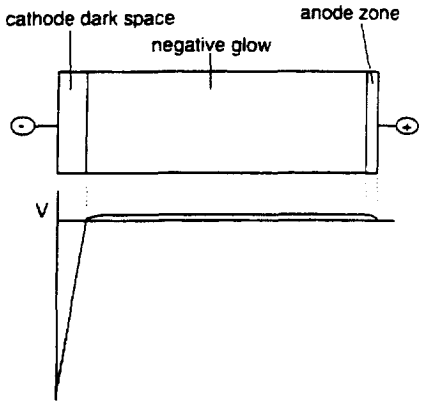

Fig. 9. Schematic representation of the three regions occurring in an analytical glow discharge and the corresponding potential distribution.

With further decrease of the distance between cathode and anode, the Faraday dark space also disappears and only cathode dark space and negative glow remain. The anode is then in contact with the negative glow. This situation is usually encountered in analytical glow discharges. In this case, the plasma carries the most positive potential and the anode zone is characterized by a negative potential fall that repels the electrons and attracts the positive ions. The situation is hence comparable with the cathode fall in the cathode dark space, but both the anode potential fall and the length of the anode zone are much smaller than in the cathode dark space. An illustration of the potential distribution in an analytical glow discharge where only cathode dark space, negative glow and anode zone are present is given in Fig. 9.

2.2.6. Influence of discharge parameters on the various regions

The occurrence of the various regions depends on the pressure, the distance between the electrodes, the potential, the electrical current, the kind of discharge gas and the kind of cathode material.

2.2.6.1. Pressure. As the pressure increases, the cathode dark space, the negative glow and the Faraday dark space are compressed towards the cathode, whereas the positive column takes up the major part of the discharge volume. Moreover, cathode dark space, negative glow and Faraday dark space cannot be so well distinguished from each other any more. A decrease in pressure has the opposite effect, i.e. the positive column and later also the Faraday dark space and negative glow will disappear in the anode. The latter is now in direct contact with the cathode dark space and a so-called 'obstructed discharge' is formed. By still lowering the pressure, the discharge will extinguish since the cathode dark space is the essential zone to sustain the discharge.

2.2.6.2. Cathode–anode distance. The effect is similar to the pressure effect. When the distance increases, the positive column spreads out towards the remaining volume and with decreasing distance, the positive column and also, but later, the Faraday dark space and negative glow will disappear in the anode.

2.2.6.3. Voltage. When the voltage increases, the cathode dark space becomes shorter. Indeed, the cathode dark space is needed to sustain the discharge. At higher voltages, the discharge will be more easily self-sustained since more ionization occurs so that a smaller cathode dark space will be sufficient. Moreover, the negative glow will become longer at higher voltages since its length is determined by the range of the electrons before they are thermalized. At higher voltages, the electrons enter the negative glow with higher energies and they will need a longer distance before being thermalized.

2.2.6.4. Current. The current has actually no influence on the length of the various regions, but it effects the radiation intensity, i.e. at higher currents, the amount of excitation increases, yielding more intense emission of radiation.

2.2.6.5. Discharge gas. The discharge gas determines the color of the negative glow and positive column (see before). Moreover it has an effect on the length of the cathode dark space, i.e. the cathode dark space is shorter when the discharge gas can be more easily ionized.

2.2.6.6. Cathode material. This influences the length of the cathode dark space. If the cathode material easily emits secondary electrons, the discharge can be more easily sustained and a shorter cathode dark space will be sufficient.

2.3. Modeling of glow discharges

2.3.1. General

To obtain a better insight in the complexity of the glow discharge and to investigate which processes play a dominant role, modeling of the glow discharge phenomena can be performed. This approach is rather new for glow discharges used in analytical applications. However, glow discharges are not only used for analytical purposes; they find applications in a variety of other fields as well: in the microelectronics industry, in laser technology, as television and computer screens (i.e. plasma display panels) and in the lighting industry (e.g. neon lamps). A substantial number of models for describing these other types of glow discharges was reported in the (plasma physics) literature [58–69]. Basically, three kinds of modeling approaches can be distinguished.

In a *fluid model* [58–62], the plasma species are assumed to be in equilibrium with the electric field, i.e. the energy they gain from the electric field is more or less balanced by the energy loss due to collisions. The species are described by continuity equations (based on the conservation laws) and transport equations (based on diffusion and migration in the electric field). This method is rather simple (although it is not straightforward to solve the coupled differential equations), but it is only an approximation, especially for 'fast species' like the electrons, which gain more energy from the electric field than they lose by collisions and are hence not in equilibrium with the electric field.

The *Boltzmann model* [2,63] describes the plasma species in a kinetic way; the energy gains and losses are explicitly calculated by different terms of the Boltzmann transport equation. This approach is therefore more correct, but it can lead to very complicated mathematical equations.

Finally, in the *Monte Carlo simulations* [64–66] the trajectory of each plasma particle is calculated explicitly based on Newton's laws, whereas the collision processes are treated with random numbers and using the cross-sections as a function of the particles' energies. When a large number of particles is followed in this statistical way, a complete picture of the glow discharge can be obtained. Since this model describes the species on the lowest microscopic level, it is the most accurate approach. Moreover, it is rather transparent and easy to understand because it makes use of basic physics. However, in order to reach statistically valid results, a large number of particles of a given kind has to be simulated (e.g. in the order of 10^4). It can, therefore, lead to long calculation times, especially for slow-moving particles.

Hence, each of these models has its advantages and disadvantages. Therefore, so-called hybrid models are often reported in the literature [67–69]: a Monte Carlo (or Boltzmann) model is applied for fast plasma species which are not in equilibrium with the electric field (like electrons), whereas a fluid approach describes the slow plasma species which can be considered in equilibrium with the electric field (like the atoms, or the ions in the negative glow).

2.3.2. Modeling of an analytical glow discharge

The models reported in the plasma physics literature deal generally only with electrons and gas (e.g. argon) ions because these species are dominant for determining the electrical characteristics of the glow discharge (i.e. they carry most of the electrical current and they determine the charge density in the plasma). Our modeling work is partly based on the models described in the literature. However, when using glow discharges for analytical purposes, interest goes primarily to the behavior of the atoms and ions of the cathode material and to metastable argon atoms (which are responsible for Penning ionization of the sputtered atoms) and excited atoms (which produce optical emission spectra). Therefore, our modeling work describes also the behavior of these species. Moreover, the analytical glow discharges operate at slightly different discharge conditions than the other types of discharges (e.g. higher voltages than the technological glow discharges used in the microelectronics industry) so that other plasma processes can come into play and have to be taken into account in the model.

A complete modeling network, existing of various submodels for the different species present in the plasma was developed [1,6,10,36–39,70–73]. To our knowledge, such a comprehensive modeling network for an analytical glow discharge has never been reported before. Table 1 presents an overview of the different species assumed to be present in the plasma, the models used to describe these species and some information about the plasma processes taken into

Table 1
Overview of the species assumed to be present in the plasma, the models used to describe these species, the relevant processes included in the models and references where more information can be found

Plasma species	Model	Processes incorporated	Reference
Thermal Ar atoms	No model	Ar atoms are assumed to be at rest and uniformly distributed throughout the discharge	
Fast electrons	Monte Carlo	Elastic collisions with Ar atoms Electron impact ionization, excitation and de-excitation of Ar atoms from the ground state and 64 excited levels Electron–electron Coulomb collisions	[36,37,70]
Slow electrons	Fluid	Transport by diffusion and by migration in the electric field	[36,37]
Ar^+ ions	Fluid	Transport by diffusion and by migration in the electric field	[36,37]
Ar^+ ions in CDS	Monte Carlo	Elastic collisions with Ar atoms, including symmetric charge transfer Fast argon ion impact ionization, excitation and deexcitation of Ar atoms from the ground state and 64 excited levels	[6,37,70]
Ar fast atoms in CDS	Monte Carlo	Elastic collisions with Ar atoms Fast argon atom impact ionization, excitation and deexcitation of Ar atoms from the ground state and 64 excited levels	[6,37,70]
Ar atoms in 64 excited states, including metastable levels	Fluid (collisional–radiative model)	Electron, fast Ar ion, fast and thermal Ar atom impact ionization, excitation and de-excitation between all levels Radiative decay between all levels Radiative Ar ion– electron recombination to all levels Three-body Ar ion–electron recombination to all levels (where the third body is an electron, fast Ar ion, fast or thermal Ar atom) Photo-ionization and -excitation from all levels. Additional loss processes for the metastable levels: • Penning ionization of sputtered atoms • Metastable–metastable collisions • Two-body and three-body collisions with Ar atoms • Diffusion and subsequent deexcitation at the cell walls	[1,10,39]
Cathode atoms	Monte Carlo	After sputtering from the cathode: thermalization by collisions with Ar atoms	[71]
Cathode atoms + ions	Fluid	Atoms: when thermalized, further transport by diffusion Ionization of the atoms by Penning ionization, asymmetric charge transfer and electron impact ionization Ions: transport by diffusion and by migration in the electric field	[38,39]
Cathode ions in CDS	Monte Carlo	Elastic collisions with Ar atoms	[38,39]

account in these models. Briefly, Monte Carlo models are used for fast plasma species which are not in equilibrium with the electric field and fluid models are applied for the slow species, which are more or less in equilibrium with the electric field. As can be seen, the electrons are split up in a fast and a slow group based on energy considerations, i.e. the fast electrons have high enough energy to produce inelastic collisions, whereas the slow electrons have too low energies and they are only important for carrying the electrical current and providing negative charge density.

All these models are coupled to each other due to the interaction processes between the species (e.g. the argon ions and the argon metastable atoms, both described with a fluid model determine the amount of ionization of the sputtered atoms by asymmetric charge transfer and Penning ionization, respectively, which gives rise to the coupling of both these models to the fluid model of the sputtered atoms and ions). The models are solved iteratively until final convergence is reached, to obtain an overall picture of the glow discharge.

2.3.3. Typical results of the models

Table 2 presents the typical results of our modeling work, together with some references where more detailed information can be found. These results are all obtained in three dimensions; they were calculated for a range of different discharge conditions [73] and for various cell types (i.e. standard cell for analyzing flat samples in the VG9000 glow discharge mass spectrometer [37,39,73], six-way cross glow discharge cell with varying lengths and diameters [74] and with either a flat or a pin cathode [75] and a Grimm-type glow discharge cell [84]). Moreover, beside using argon as discharge gas, the models have also been applied to a glow discharge operating in neon [85]. The various plasma quantities depend of course on discharge conditions, cell geometry and discharge gas and the given values for these quantities should therefore only be considered as orders of magnitude.

To test the validity of the modeling work, the calculation results have to be compared with experimental data. Such a comparison was carried out already for a number of plasma quantities, as is illustrated in the table. As an example, Fig. 10(a) presents the two-dimensional sputtered tantalum atom density profile, obtained by the modeling calculations. The position of the cathode is indicated with the black line with z and r equal to zero. The calculated density is low close to the cathode, it increases and reaches a maximum at a few millimeters from the cathode whereafter it decreases gradually towards the cell walls. To check this modeling result, the tantalum atom density profile was measured with laser-induced fluorescence at exactly the same discharge conditions and for the same cell geometry and the result is illustrated in Fig. 10(b). The calculated and experimental profiles are in very good agreement with each other, both qualitatively and quantitatively. Only at $z = 0$ are the modeling results slightly different, which is due to some simplifications in the model (i.e. a cell wall was assumed at $z = 0$, whereas in reality an insertion

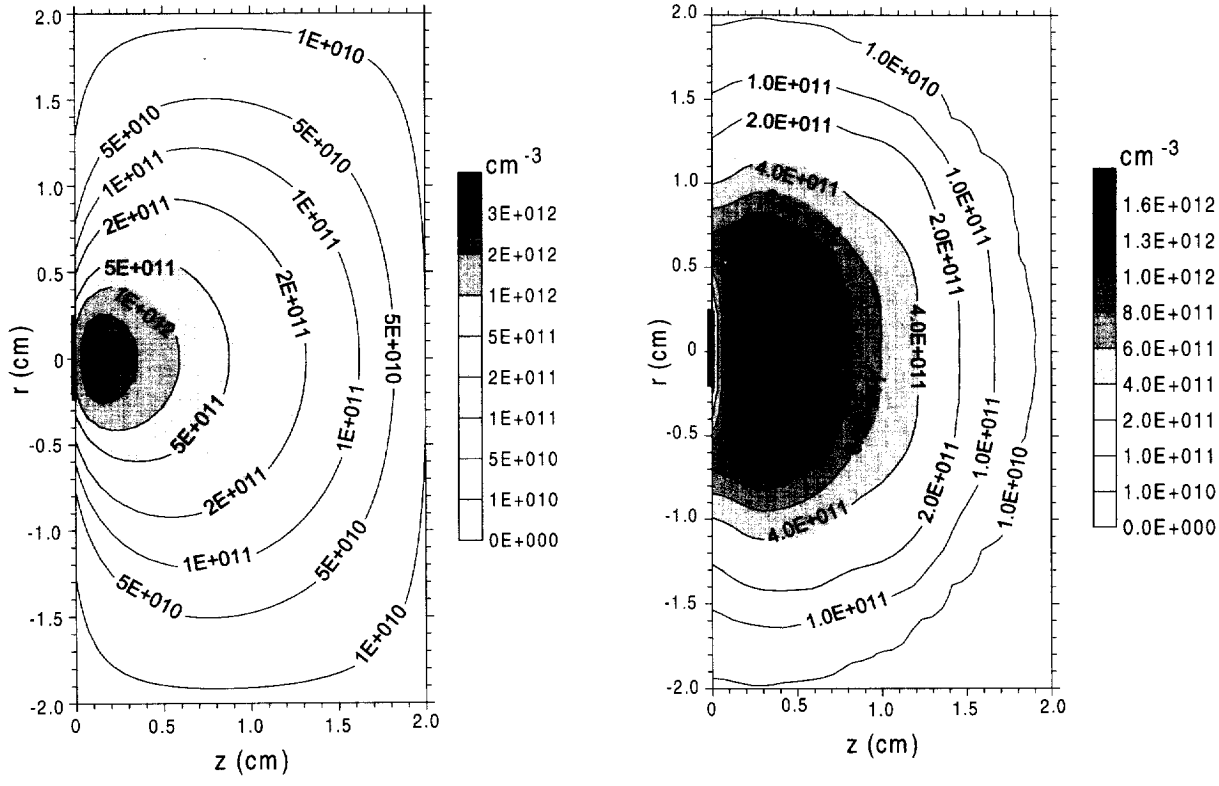

Fig. 10. Sputtered tantalum atom density profiles, obtained by the modeling work (a) and by laser induced fluorescence measurements (b) at 1000 V, 1 Torr and 2 mA. Reprinted from Ref. [78] with permission of Elsevier Science.

Table 2
Typical results of our models and comparison with experimental data if available; the references where more information can be found are also included

Calculated quantities	Reference	Comparison with experimental data	Reference
Electrical current as a function of voltage and pressure	[6,73]	Satisfactory agreement with experimental current–voltage–pressure characteristics, measured with a GDMS ion source	[6,73]
Three-dimensional potential distributions	[36,37,73]	—	
Three-dimensional axial and radial electric field distributions	[36,37,73]	—	
Value of the plasma potential: a few volts	[36,37,73][74,75]	—	
Lengths of the different regions	[6,36,37,73][74,75]	Length of CDS as function of pressure and current agrees well with empirical formula of Aston [76]	[6,73]
• Cathode dark space (CDS): a few mm • Anode zone (AZ): less than a mm • Negative glow (NG): rest of the discharge (e.g, a few cm)			
Three-dimensional density profiles of			
• Argon ions: 10^{10}–10^{12} cm^{-3}	[36,37,73]	—	
• Fast argon atoms: approximately 10^{11}–10^{12} cm^{-3} (only in CDS)	[70,73]	—	
• Argon metastable atoms: 10^{9}–10^{12} cm^{-3},	[1,10,39,73]	Reasonable agreement with laser induced fluorescence (LIF) measurements	[77]
• Other argon excited levels: 10^{7} (and lower)–10^{11} cm^{-3}	[10]	—	
• Fast electrons: 10^{7}–10^{8} cm^{-3},	[36,37,70,73]	—	
• Thermalized electrons: 10^{10}–10^{12} cm^{-3}	[36,37,73]	—	
• Atoms of the cathode material: 10^{12}–10^{13} cm^{-3},	[38,39,73]	Good agreement with LIF and atomic absorption measurements	[78]
• Ions of the cathode material: 10^{8}–10^{11} cm^{-3} (thermalized argon atoms are assumed to be uniformly distributed throughout the discharge)	[38,39,73]	Reasonable agreement with LIF measurements	[78]
Ion fluxes of argon and cathode ions at the exit slit of the cell towards the mass spectrometer	[74,75]	Ratio is in qualitative agreement with ratios in the mass spectra of GDMS	[74,75]
Ionization degrees of • Argon atoms: $< 0.001\%$–0.01%, • Cathode atoms: 0.001%–a few %	[38,39,73]	For cathode atoms good agreement is reached with the LIF results (see above)	[78]
Three-dimensional energy distributions and mean energies of:			
• Electrons (maximum mean energy at end of CDS is approximately 50% of discharge voltage)	[36,70,73]	—	
• Argon ions (maximum mean energy at cathode is approximately 10%–15% of discharge voltage)	[70,73]	Energy distribution at cathode is in satisfactory agreement with measurements using a double focusing mass spectrometer	[79]
• Fast argon atoms (max. mean energy, at cathode, is approximately 3% of discharge voltage)	[70,73]	—	

Table 2 Continued

Calculated quantities	Reference	Comparison with experimental data	Reference
• Cathode ions (maximum mean energy at cathode is approximately 60%–80% of discharge voltage).	[38,39,73]	Energy distribution at cathode is in satisfactory agreement with measurements using a double focusing mass spectrometer	[79]
Information about collision processes:			
• Three-dimensional collision rates of the different collision processes of electrons, argon ions and fast argon atoms and relative importances of these collision processes	[6,36,37,70,73]	—	
• Relative contributions to the ionization of argon: by electrons (approximately 85%–95%); fast argon ions (approximately 1%–4%); fast argon atoms (approximately 3%–14%); metastable–metastable collisions and two-step ionization from the metastable levels ($< 1\%$)	[6,37,73]	—	
• Three-dimensional rates of Penning ionization, asymmetric charge transfer and electron impact ionization and relative contributions to the total ionization of sputtered atoms: Penning ionization (approximately 30%–90%); asymmetric charge transfer (approximately 10%–60%); electron impact ionization (a few %)	[38,39,73]	—	
• Three-dimensional rates and relative contributions of the various populating and depopulating processes (see Table 1) of the metastable and other excited argon levels	[1,10,39,73]	—	
Information about sputtering:			
• Sputtering (erosion) rates at the cathode (approximately 0.1–30 μm/h)	[38,39,70,80]	Good agreement with values measured in a typical GD source for MS	[81]
• Thermalization profiles of the sputtered atoms	[71,73]	—	
• Amount of redeposition on the cathode by backscattering (3%–8%) or backdiffusion (40%–60%)	[71,73,80]	—	
• Relative contributions of argon ions, fast argon atoms and cathode ions to the sputtering process (i.e. approximately 20%–30%, 70% and 0.1%–10%, respectively)	[38,39,70,73]	—	
• Two-dimensional crater profiles due to sputtering at the cathode	[73,80]	Good agreement with profiles obtained in a typical GD source for MS	[81]
Emission spectra and emission profiles due to radiative decay from the excited levels	[10]	Good agreement with spectra from the literature	[82]
Prediction of variations in relative sensitivity factors (RSF) for GMS	[18]	Compared with RSFs from the literature	[83]

probe is used as cathode and the glow discharge chamber also extends to negative z-values for $r >$ 2.5 mm). The absolute values of calculated and experimental profiles differ by only a factor of about 2. The tantalum atom density profiles have also been measured for the same conditions by a combination of laser-induced fluorescence (to obtain the relative profiles) and atomic absorption spectrometry (to put

an absolute value on the profile) and the results differed from the complete laser-induced fluorescence profile [Fig. 10(b)] by a factor of 3. Hence, this is the expected error for the experimental profiles (and it may be more if the good agreement between both experimental results is only coincidence). Therefore, it can be concluded that the calculated and experimental profiles are similar to each other within the experimental uncertainties.

For more detailed information about the modeling results and a comparison with experimental data, the reader can consult the cited references. In general, satisfactory agreement between calculated and experimental results was obtained, which shows that the models present already a realistic picture of the glow discharge.

2.4. Plasma diagnostic study of glow discharges

As already mentioned, a better understanding of glow discharges can also be achieved by measuring the characteristic plasma quantities, which is called 'plasma diagnostics'. A large number of experimental set-ups for measuring different quantities was described in the literature (see also Ref. [86]). Again, glow discharges used for other than analytical purposes (e.g. technological purposes) were studied more thoroughly than analytical discharges and a lot of information is, therefore, reported in the plasma physics literature. In the following, the most well-known plasma diagnostic experiments carried out on glow discharge plasmas will be briefly discussed.

2.4.1. Langmuir probe measurements

These are undoubtedly the most widely used of all plasma diagnostic techniques for glow discharges [87–93]. The technique consists of inserting one or more wires into the plasma, to which a known voltage is applied. By changing the voltage at the probe and recording the corresponding current, the current–voltage characteristic of the probe is obtained, from which in principle the following plasma properties can be deduced: the slow electron and positive ion number densities, the value of the plasma potential, the electron temperature(s) and electron energy distribution. A typical current–voltage characteristic is illustrated in Fig. 11. Although the construction of the Langmuir probe and the recording of the current–voltage characteristics are relatively straightforward, the data analysis for recovering the actual plasma quantities is very complex. A general theory valid for all plasma parameters and probe shapes (cylindrical, spherical or flat) does not exist; instead, there are different sets of approximate equations, corresponding to different limiting regions of plasma parameters. Moreover, the Langmuir probe must be very small, in order to avoid disturbance of the plasma, otherwise the real plasma is not observed, but only the disturbed region around the probe and the measured quantities do not reflect the real plasma. Due to the approximate nature of calculating the plasma properties and due to the possible disturbance of the plasma by the probe, the obtained results are, to our opinion, subject to considerable uncertainties.

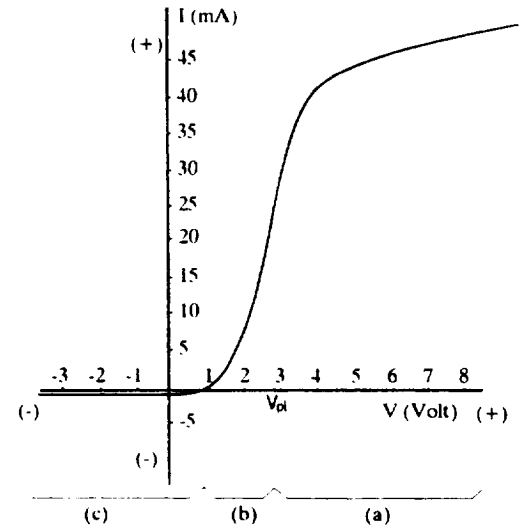

Fig. 11. Typical I–V characteristic of Langmuir probe measurements: (a) electron saturation region; (b) electron retardation region; (c) ion saturation region. V_{pl} = plasma potential. Reprinted from Ref. [90] with permission of Elsevier Science.

2.4.2. Optical emission spectrometry

From the intensities, intensity ratios or the widths of optical spectral lines, information can be obtained about electron densities and different temperatures in the plasma, i.e. the gas temperature, excitation, ionization and rotational temperatures. Optical emission spectrometry is a noninvasive plasma diagnostic method, which is one of its major advantages compared with Langmuir probe measurements.

Excitation temperatures are obtained, based on the assumption that the glow discharge plasma is in local thermal equilibrium (LTE), i.e. the populations of atoms, ions or molecules of the species at the different energy levels follow a Boltzmann distribution. The intensities of a large number of spectral lines are measured. If $\ln(I_{qp}\lambda_{qp}/g_qA_{qp})$ is plotted against E_q (where I is the intensity of the spectral line, λ is its wavelength, A is the Einstein transition probability and g and E are the statistical weight and excitation energy of the upper level, respectively), a straight line will result (a so-called Boltzmann plot), the slope of which yields the excitation temperature. An example of a Boltzmann plot is presented in Fig. 12. A large number of such measurements on glow discharges was reported in the literature [90,94–98] since they are relatively easy to perform. Nevertheless, the experiments can be time-consuming because a large number of spectral lines has to be measured to define the excitation temperature. Care has to be taken that the spectral lines are not subject to interferences. Moreover, the glow discharge is generally not in LTE and therefore, the obtained results do actually not have the real physical meaning of excitation temperature.

Similarly, *rotational temperatures* can also be obtained from a Boltzmann plot, as was demonstrated in Ref. [98] for N_2^+. Since the energy differences between rotational energy levels are small and since rotational relaxation is very fast, the excited rotational states are in equilibrium with the kinetic energy of the molecules. Therefore, the rotational temperatures can be considered as a reasonable approximation for the kinetic gas temperature.

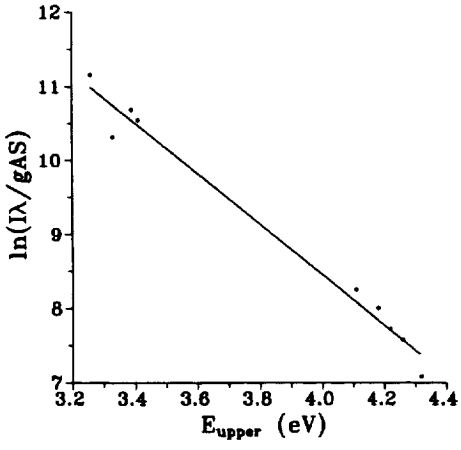

Fig. 12. Typical Boltzmann plot for FeI lines, measured with a Grimm-type source at 550 Pa and 1000 V.

The *ionization temperature* can, in principle, be estimated from spectral lines of atoms and ions of the same species [e.g. Ar(I) and Ar(II)] [90,99]. However, this determination is also based on the assumption of nearly LTE and it is therefore not very suitable when the glow discharge is not in LTE.

The *gas temperature* can be obtained from the Doppler broadening of atomic spectral lines, as was demonstrated for some Ar(I) lines in Refs [97,100] for a Grimm-type glow discharge. Indeed, for Ar(I) lines, Stark broadening seems to be negligible even at high electron number densities and the line shape is then determined by Doppler broadening only.

However, hydrogen lines are much broader in a glow discharge owing to the Stark effect and the shape of these lines can be used to determine *electron number densities* in the plasma. This was demonstrated in Ref. [97] for the hydrogen H_β line in a Grimm source. In Ref. [100] the hydrogen H_β line was found to be too wide for the spectral instrumentation and a He(I) line was therefore used for measuring the Stark broadening and obtaining the electron number density in a Grimm source

Moreover, from the investigation of certain emission line profiles, information can be obtained about the excitation mechanisms of certain levels. Jelenak and coworkers studied a number of Ar lines to estimate the effect of cascading from upper levels to 2p levels [101], whereas in some other papers the occurrence of asymmetric charge transfer for the ionization of specific elements was demonstrated by looking at the intensities of certain emission lines [19–23].

2.4.3. Mass spectrometry

The ion peaks in the mass spectrum can sometimes yield information about ionization processes in the plasma. Indeed, in Ref. [102], the Cu^+ ion current was measured with GDMS in an RF glow discharge and its behavior as a function of RF power and gas pressure was found to be proportional with the product of the copper atom and neon metastable atom densities, both determined by atomic absorption spectrometry. This suggested that Penning ionization is a dominant ionization mechanism of the sputtered

copper atoms. A similar study was performed in Ref. [103] by the combination of mass spectrometry and optogalvanic spectroscopy. A tunable laser served to depopulate the metastable atom population and the effects were followed with both optogalvanic spectroscopy and mass spectrometry, to investigate the role of Penning ionization in the plasma. Furthermore, the presence of certain cluster peaks in the mass spectra makes it possible to speculate about production and/or destruction mechanisms of clusters in the plasma.

However, mass spectrometry cannot give direct information about plasma properties and certain interpretations are always required. This can sometimes lead to wrong conclusions, as was pointed out by Steers [20] concerning the relative importance of Penning ionization and asymmetric charge transfer. Indeed, in their early mass spectrometric studies [16], Coburn and Kay considered Penning ionization as the most important ionization mechanism and they ruled out the possibility of asymmetric charge transfer because they assumed that in the latter process the analyte ions are formed in the ground state so that the energy difference with the gas ion levels was too large. Mass spectrometry can, indeed, give no information about excited states, but Steers demonstrated by optical emission spectrometry that the analyte ions are mainly formed in excited states so that the energy difference with gas ion levels is much smaller and asymmetric charge transfer can occur.

Recently, a compact mass spectrometer was reported in the literature [104] for ion species analysis in one single step instead of the usual two steps (i.e. ion extraction and mass filtering). The instrument is made small enough to be directly introduced in most plasma discharges for in situ diagnostic studies, which may lead to promising experiments in the future.

Finally, it is worth mentioning that the double focusing VG9000 glow discharge mass spectrometer (VG Elemental, Thermo Group) was used recently to measure energy distributions of ions bombarding the cathode of a glow discharge cell [79]. The energy scans were recorded by varying the acceleration voltage and keeping the magnetic field constant. It was found that argon ions are characterized by a decreasing energy distribution towards high energies, whereas the ions of the cathode material have a pronounced peak at maximum energy. This was also observed in Ref. [105] where a similar study was carried out for a hollow cathode glow discharge lamp with a double focusing Cameca IMS 3f mass spectrometer. In the latter work, it was suggested that interfering signals from the discharge gas ions may be significantly reduced by adjusting the mass spectrometer to sample only the high-energy ions of the cathode material (material to be analyzed). Other papers in the literature report the measurement of ion energy distributions by using a quadrupole mass spectrometer in combination with an electrostatic energy analyzer [106–110].

2.4.4. Retarding field analyzer to measure energy distributions

Energy distributions of ions in a glow discharge can also be measured with a retarding field analyzer, as is illustrated, for example, in Refs [111,112]. This technique has also successfully been applied to the measurement of electron energy distributions in a helium discharge, which is a very important plasma property [113]. Briefly, in the latter case the analyzer consists of a sampling orifice followed by a metal screen having a certain circular aperture and a Faraday collector situated immediately behind the aperture. A negative potential is applied to the retarding screen so that only electrons with sufficiently high energies can pass through the aperture and can reach the Faraday collector. By gradually decreasing the negative potential, electrons with lower energies can pass and hence the total energy distribution can be recorded in this way. It was shown in Ref. [113] that the resulting electron energy distributions are clearly non-Maxwellian, but are characterized by a dominant group of low-energy electrons and a small peak at maximum energy, corresponding to electrons which have not undergone any collision in the discharge, which agrees well with our modeling results [36,73].

2.4.5. Atomic absorption spectrometry

Atomic absorption spectrometry (AAS) can be carried out to obtain absolute number densities of the plasma species. This is demonstrated, among others, by Ferreira and coworkers for the argon metastable atoms and the sputtered atoms in a Grimm glow discharge [114,115] using a hollow cathode lamp as primary source. In Ref. [116], similar measurements

were made for the argon metastable atoms in a microwave boosted Grimm source, but the primary source was a diode laser.

A disadvantage of conventional AAS experiments is that accurate knowledge of the absorption coefficient is required, or that calibration with known standards has to be carried out. This drawback is overcome by a rather new atomic absorption technique, called 'concentration modulated absorption spectrometry' (COMAS) [117]. Two laser beams (or the vertical and horizontal components of the same laser beam) are sent through the absorbing medium (e.g. the glow discharge). The first beam, called pump beam, is modulated. When the pump beam is 'on', it is absorbed in the glow discharge and causes hence perturbation in the concentration difference between the two states coupled by the incident radiation. The second beam, called the probe beam, is sent through the discharge and will not be absorbed to a large extent because the concentration of the lower state is depleted. However, when the pump beam is turned 'off', no concentration perturbation occurs and the probe beam will be more absorbed. The difference in intensity of the probe beam after passing through the absorbing medium is measured and the gain created on the probe beam provides a direct measure of the concentration of the absorber. Because the experiment is on a relative scale (i.e. the intensity difference between the 'on' and 'off' situation is measured), there is no need for calibration using a known concentration or for an accurate knowledge of the absorption coefficient. This technique was developed by Jones and coworkers [117] and was successfully applied to sputtered lithium atoms in glow discharges by Mason and collaborators [118].

2.4.6. Laser-induced fluorescence spectroscopy

Conventional AAS measurements with nonlaser sources are, in principle, not well-suited to perform laterally resolved three-dimensional density measurements since only integrated values are obtained. For this purpose, laser-induced fluorescence (LIF) spectroscopy is a better technique.

In Refs [77,78], complete three-dimensional density profiles of argon metastable atoms and of sputtered tantalum atoms and ions in a glow discharge were measured with LIF. The absolute values were obtained by properly calibrating the gain of the electronics and the response of the monochromator and photomultiplier tube. Moreover, for the tantalum atoms, a combination of LIF and AAS measurements was carried out as well: the LIF experiment yielded the three-dimensional relative density profiles whereas the AAS measurement allowed to put an absolute number on these profiles. The results of the complete LIF experiments (with proper calibration of the instrumentation used) and the combined LIF and AAS measurements were in satisfactory agreement with each other, as well as with modeling results [78] [see also Fig. 10(a and b)]. Fig. 13 shows a schematic overview of the combined LIF and AAS experimental set-up.

In the authors' opinion, LIF spectroscopy is a very powerful plasma diagnostic technique for measuring absolute densities of the plasma species. Moreover, apart from density measurements, LIF can also be used to measure fluorescence lifetimes, absorption line widths, quantum efficiencies and velocity distributions.

2.4.7. Thompson scattering

Another technique which makes use of a laser as primary source, is Thompson scattering. It occurs when an electromagnetic wave interacts with charged particles. Since the scattered radiant power is inversely related to the square of the charged particle mass, scattering of the electromagnetic wave occurs mainly from electrons. The electrons have rather high velocities in the glow discharge; hence, the light scattered by the electrons will be strongly Doppler shifted and the Doppler shift will increase with the velocity of the electrons. From the collection of the complete Doppler shift spectrum produced by the electrons, the electron velocity (and energy) distribution can be deduced. Moreover, since the integrated intensity under the Doppler shift spectrum is proportional to the total number of electrons, the electron density can also be obtained from this experiment.

This method does not require LTE conditions in the plasma or a Maxwell energy distribution of electrons. Furthermore, it is a noninvasive method. Finally, when a pulsed laser is used as the light source, the latter can be focused to a small region in the plasma and the observation direction and incident laser beam can overlap at only a single point in the discharge, which gives rise to both high spatial and temporal

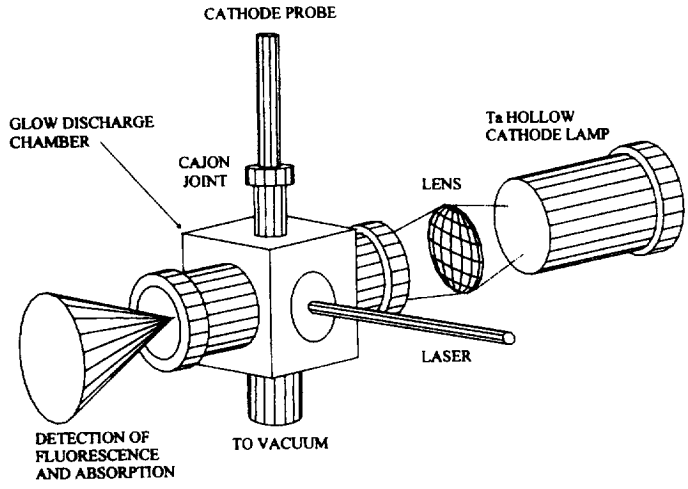

Fig. 13. Schematic overview of the experimental set-up for the combined LIF and AAS experiments. Reprinted from Ref. [78] with permission of Elsevier Science.

resolution. This technique was successfully used to inductively coupled plasmas (ICP), e.g. by Hieftje and coworkers [119,120], but to our knowledge, it has not yet been applied to glow discharges since it is practically restricted to electron densities above 10^{11} cm^{-3} [121].

2.4.8. Rayleigh scattering

This technique is comparable with Thompson scattering, except that the laser light is now scattered from relatively large particles (e.g. Ar atoms). The ideal gas law yields a relationship between the gas density and the gas temperature (i.e. $n = N/V = p/kT$, where n is the gas atom density, N and V are the total number of gas atoms and the volume, respectively, p and T are the gas pressure and temperature and k is the Boltzmann constant). Since the intensity of the scattered laser light is linearly related to the gas atom density, the gas temperature can be determined. Like Thompson scattering, this technique was applied to measure gas temperatures in ICP's [119,120], but we are not aware of similar experiments on glow discharges.

2.4.9. Stark experiments for electric field measurements

Finally, a number of papers has recently been published in the literature, describing the measurement of the electric field distribution in glow discharges by means of Stark spectroscopy [122–125]. Briefly, the energy levels of hydrogen and hydrogen-like emitters in an external electric field are split due to the Stark effect. Consequently, the spectral lines emitted as a transition between such split levels consist of a number of components and from the peak-to-peak separation between these components, the electric field strength can be deduced.

3. Analytical applications of glow discharges

As mentioned before, glow discharges are useful as spectroscopic sources for a variety of analytical techniques (see Fig. 14), i.e. mass spectrometry (GDMS), optical emission spectrometry (GD-OES), atomic absorption spectrometry (GD-AAS) and atomic

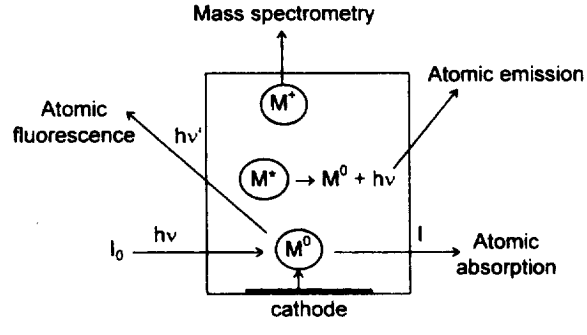

Fig. 14. The glow discharge as a versatile analytical tool.

fluorescence spectrometry (GD-AFS). Analytical applications in these different fields will be discussed and some new developments of glow discharges in hybrid analytical constructions will be reported. However, first a brief overview will be given of the various types of analytical source configurations and the different electrical operation modes.

3.1. Glow discharge analytical source configurations

As mentioned in Section 1, the glow discharge is created by two electrodes inserted in an (inert) gas. For analytical purposes, these two electrodes are generally mounted in five different geometries (see Fig. 15).

(1) The *coaxial cathode* is the most widely used source configuration in GDMS applications. Samples can be made in pin-form (with a few millimeters exposed to the discharge) or in disk form (partly shielded so that only the top part is exposed to the discharge). The sample acts as cathode whereas the anode is formed by the cell body itself.

(2) The *planar diode* is the simplest analytical source. It is used for analyzing samples in disk form. The cathode (sample) and anode are in parallel configuration and are placed inside a tube.

(3) In the *hollow cathode lamp*, the cathode forms a cavity rather than a pin or disk. It can be considered as three planar cathodes placed so close to each other that their negative glow regions coalesce into a single negative glow. This results in increased sputtering and ionization/excitation, yielding a much better analytical sensitivity. A disadvantage of this source is the extensive machining required to make hollow cathodes from metal samples. Because most of the sputtering occurs at the cathode base, studies were performed using a disk sample as the base of the cathode. Hollow cathode devices are particularly used as sources for optical emission spectrometry. Moreover, the high radiation intensity emitted by this source, makes it attractive as primary source for atomic absorption or fluorescence spectrometry.

(4) In the *hollow cathode plume*, the sample is mounted in the base of the hollow cathode, in which also an orifice is made. A highly energetic flame-like plume, where excitation and ionization processes occur, is ejected through this hole. Due to the high atom population, this geometry is also characterized by a high sensitivity. The physical processes of this

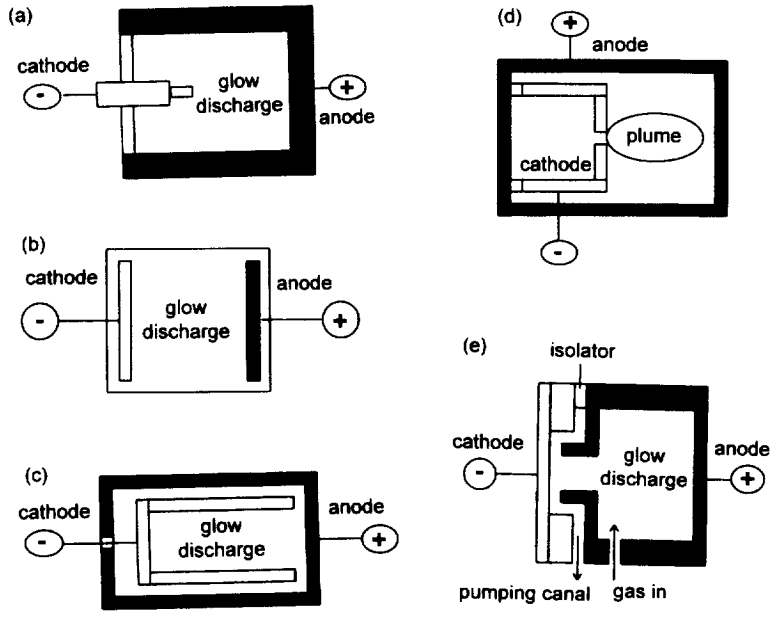

Fig. 15. Different glow discharge source configurations: (a) the coaxial cathode; (b) the planar diode; (c) the hollow cathode lamp; (d) the hollow cathode plume; and (e) the Grimm-type glow discharge.

source are not fully understood, but the plume is believed to arise from pressure and field effects due to the special construction of the cathode orifice.

(5) The *Grimm configuration*, named after its inventor in 1968 [126], is extensively used in GD-OES and forms the basic design for all commercial emission instruments. The cell body (anode) approaches the cathode very closely (at a distance smaller than the length of the cathode dark space) so that the discharge is constricted to a well defined part of the sample surface. It is therefore called an 'obstructed discharge'. The Grimm configuration can, however, only be used for flat samples. This type of source is particularly useful for in-depth analysis since the flat sample is ablated layer by layer.

3.2. Glow discharge electrical operation modes

The simplest and cheapest operation mode is the *direct current* (DC) mode. Voltages are typically in the order of 500–1500 V, yielding electrical currents ranging from a few to several hundreds of milliamps depending on the pressure in the cell and the discharge configuration. This type of discharge mode is the oldest one and the most widely used in glow discharge applications. However, it has the serious drawback of not being able to analyze nonconducting samples directly. Indeed, since in a glow discharge the sample to be analyzed acts as the cathode, which is sputter bombarded by positive ions, it must be conducting. If not, the surface would be charged up, preventing the positive ions from further bombarding. Due to this drawback of the DC mode, attention is being drawn during the latest decade to the *radio frequency* (RF) operation mode.

The *radio frequency* mode is indeed able to analyze nonconductors directly since the positive charge accumulated during one half-cycle will be neutralized by negative charge accumulation during the next half-cycle so that no charging up occurs. Operation with RF-power of a glow discharge using a nonconducting sample yields a negative DC bias voltage on the sample surface. Indeed, during the half-cycles in which the nonconducting electrode is positive, surface charging will occur much faster than in the half-cycles in which the electrode is negative due to the much higher mobility of the electrons compared with the positive ions. This self-bias phenomenon permits the establishment of a time-averaged cathode and anode in the glow discharge so that sputter bombardment of positive ions on the cathode is still possible. Since the electrons try to follow the RF electric field, they oscillate between the two electrodes and spend more time in the plasma before they are lost, which results in a higher ionization efficiency. This leads to the second advantage of RF discharges, i.e. they can be operated at much lower pressures for the same current than DC discharges, which is interesting for reducing redeposition and spectral interferences. The RF-powered GD sources were introduced for the direct analysis of nonconductors with GDMS in the 1970s by Coburn and Kay [127] and by Donohue and Harrison [128]. However, it took until the late 1980s before RF GDMS really broke through [129]. Since then, extensive work was performed in this field [130–142]. RF discharges were combined with optical emission spectrometers [135,142] and different types of mass spectrometers (i.e. quadrupole mass spectrometers [129,133,141], a Fourier transform mass spectrometer [131], an ion trap mass spectrometer [132], a time-of-flight system [136] and two sector-based mass spectrometers [134,138]), but up to now there is no commercial RF-GDMS instrument and only one commercial RF-GD-OES instrument (JY 5000 RF, Jobin Yvon) available.

The third mode of operation of a glow discharge is the *pulsed* mode, which can be employed in combination with a conventional DC or with an RF glow discharge. Voltage and current are applied only during short periods of time (generally milliseconds range). Hence, compared with a normal DC discharge, higher peak voltages and peak currents can be obtained for the same average power. Therefore, more highly-energetic gas ions can be produced, yielding more sputtering, a higher concentration of analyte atoms in the plasma and hence better analytical sensitivity. In addition to the better sensitivity, the pulsed mode has a second advantage for mass spectrometry, i.e. the analytically important ions and the interfering ions are formed during a different time in the pulse. By coupling this 'time-resolved' production of ions to a time-resolved detection, spectral interferences in the mass spectrum can be reduced [143]. Moreover, the construction of a pulsed dual discharge system allows for simultaneous analyses with two electrodes, rendering the possibility of in situ calibration of an unknown

sample against a reference standard [144]. Gated detection of atomic emission from a pulsed RF glow discharge was also reported to improve the analytical sensitivity and to reduce spectral interferences [145]. Also in glow discharge atomic absorption and fluorescence spectrometry, background-free analytical measurements during the discharge-off portion of the cycle were reported [146]. Recently, Harrison and coworkers introduced the microsecond pulsed glow discharge as source for atomic emission, absorption, fluoresence and mass spectrometry [147,148]. Due to the still higher peak currents and voltages which can be obtained during the short pulses, this source has still a better analytical sensitivity.

3.3. Analytical applications of glow discharges

3.3.1. Glow discharge mass spectrometry (GDMS)

The glow discharge was known as an ion source in mass spectrometry for more than 60 years. Gas discharges were indeed already used in the 1920s and 1930s as ion sources in the first mass spectrographs of Aston and Bainbridge [149,150]. However, the early popularity was followed by a decline into relative obscurity during the next 30 years, due to the development of the electron impact ion source and later the spark and arc discharge sources. In the early 1970s, the glow discharge was brought back to the attention of mass spectroscopists as ion source for the analysis of solids (both in DC and RF mode) by Coburn et al [16]. Later, in particular, Harrison and coworkers were pioneers in the development of modern GDMS [151–153].

To date, all common mass analyzers were explored for use in GDMS. The first commercially available GDMS instruments used a double-focusing (magnetic sector) mass analysis system, permitting the acquisition of high-resolution spectra with high sensitivity [154]. Modern GDMS began, however, with quadrupole-based mass analyzer systems, which were employed for fundamental and development research of GDMS [152,155] and this research resulted finally in the commercial availability of a quadrupole GDMS system [156]. Promising results have also been obtained from the coupling of a glow discharge to ion trap mass spectrometric systems [157], double and triple quadrupole instruments [158], time-of-flight mass spectrometers [136] and Fourier transform mass spectrometers [131,159]. The commercial GDMS systems available at present employ, however, only double-focusing and quadrupole-based mass spectrometers. Typical working conditions for GDMS are 1–5 mA, 800–1500 V and 0.2–2 Torr. Detection limits of magnetic sector GDMS are in the ppb region.

GDMS permits the analysis of a broad range of sample types. The most important applications are found in the bulk analysis of metals, but semiconductors, nonconductors, thin films solutions and gaseous samples can in principle be analyzed as well.

Bulk metals are the most interesting sample types for GDMS. Due to the low detection limits for almost all elements of the periodic table, it is of particular interest for analyzing high-purity metals, like aluminum, gallium, titanium, copper, platinum, etc. [160]. In addition, metallic alloys can be easily analyzed by GDMS [83,161–163]. Isotope ratio measurements on metals can also be carried out with GDMS, as is described in Ref. [164]. A common problem in GDMS are the spectral interferences by various types of cluster ions, many of which, but not all, can be resolved with a high mass resolution instrument. As mentioned before, a paper has recently been published reporting the suppression of cluster and discharge gas interferences by sampling from a reversed hollow cathode ion source because it was found that the analyte ions are characterized by a peak at high energy, whereas argon ions and cluster ions possess a peak at low energy. By sampling only high-energy ions, the argon ion and cluster ion interferences could be suppressed [105]. Another recent paper makes use of these clusters for quantification; indeed, argides, dimers and doubly charged analyte ions are sometimes less disturbed by interferences and can therefore better be employed for quantification than singly charged analyte ions [165].

To calculate concentrations of trace elements in the sample, the ion beam ratio method can simply be used. The assumption is made that the ratio of the ion current for any one isotope with respect to the total ion current (except the signal arising from the discharge gas ions) is representative for the concentration of that isotope in the sample. Since the ion signal for the matrix is generally large compared with the individual trace species, especially for a high purity metal or semiconductor, the matrix ion current

is in good approximation equal to the total ion current and the matrix atoms can be assumed to have a concentration of 100%. Since this method cannot correct for the variation in analytical sensitivity among different elements, it provides only semi-quantitative results, i.e. accuracies of a factor of 2–3. Real quantitative results require that differences in elemental sensitivities be characterized using standards similar to the material under study. This characterization generates relative sensitivity factors (RSF) that can be employed to correct the measured ion beam ratios. Since RSFs vary only slightly between matrices of the same general composition, exact matrix matching is not required to yield quantitative results with accuracies of 15%–20% [162]. The RSF method of quantification is the most widely employed in GDMS. Generally, the RSFs of different elements in GDMS lie within one order of magnitude (see, for example, Fig. 16, [162]), which makes GDMS a technique with rather uniform sensitivity for most elements. Experimental RSFs were reported for different kinds of matrices [83,161,166]. Further, some empirical models based on fitting parameters were developed to predict RSFs [83,166,167]. In Ref. [166] it was found that the theoretically calculated RSF values correlated better with the experimental ones when 1% H_2 was added to the argon discharge gas.

Semiconductors can also, in certain forms, serve directly as cathode samples in GDMS because they exhibit certain allotropic forms that conduct electricity to a certain degree, in spite of their generally nonmetallic chemical activity. Their concentrations have to be known very accurately since impurities even at extremely low concentration levels can seriously alter the semiconductor properties. A few applications of the analysis of semiconductors by GDMS were reported in the literature [160].

Since the sample in the glow discharge acts as the cathode bombarded by positive ions, the concept seems to restrict the applications of GDMS to the analysis of electrically conducting materials because nonconductive materials would be charged up. However, the problem of analyzing *nonconductors* can be overcome by using RF discharges, as mentioned before [131–134,139]. Nevertheless, the calibration of this method may be hampered in practice by different sample thicknesses. In a DC discharge, nonconductors can also be analyzed when applying certain modifications. Two methods are reported in the literature. The first exists in mixing the nonconducting

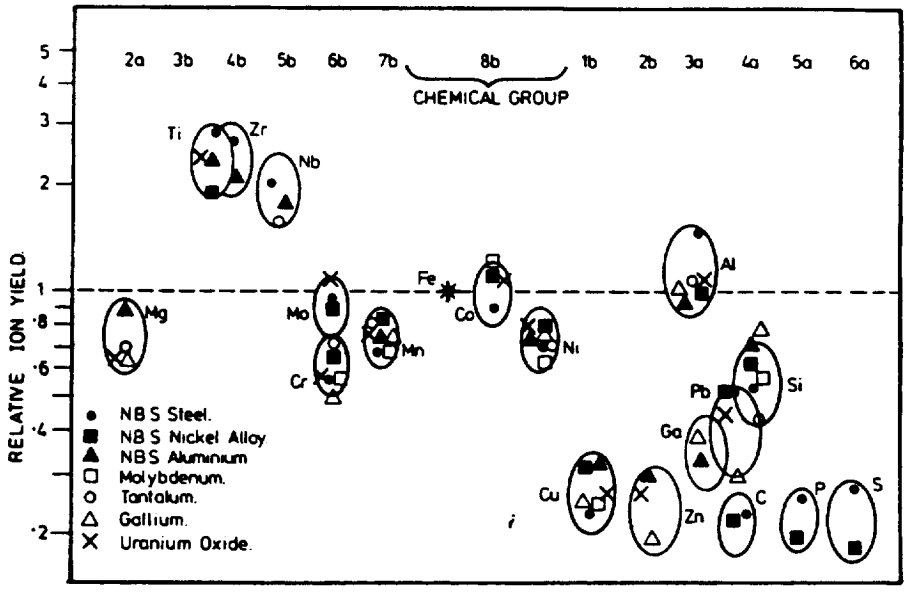

Fig. 16. Relative ion yields for various elements in different matrices, measured with the VG9000 glow discharge mass spectrometer. Reprinted from Ref. [162] with permission of Springer, Berlin.

sample as a powder with a conductive binder (Cu, Ag and Ga) and pressing it into an electrode. This method is generally well-established, as can be seen from the large number of articles in the literature [161,168,169]. However, in addition to the increase in sample preparation time compared with the direct analysis of conducting solids, the mixing with the conductive matrix can introduce contaminations. Other problems arise from the trapping of water vapor and atmospheric gases in the sample during the compaction process. In addition, the time to reach steady-state conditions with a composite cathode can be prohibitively long. The second approach is the use of a metallic secondary cathode diaphragm in front of the flat nonconducting sample surface [170,171]. As a result of the redeposition of a part of the sputtered metal atoms from the secondary cathode, a very thin conductive surface is formed on the nonconductive material. The sampling depth is large enough (approximately 5 Å) to allow atomization of the nonconducting sample as well. This method has recently been applied to the analysis of a variety of sample types, ranging from atmospheric particulate matter (aerosols), to ceramics, glass, radionuclides in sediment samples and even polymers [172–176].

The concept of sputtering in a glow discharge implies that the sample is being eroded 'layer after layer'. It is therefore possible to perform trace analysis of successive layers as a function of depth (i.e. depth-profiling). Although depth-profiling is more typically performed in glow discharge optical emission spectrometry (see below) some applications of GDMS can be found in the literature as well [177,178]. Since transient signals have to be monitored (intensity as a function of time), quadrupole-based mass spectrometers are preferable due to their fast scanning capability.

Although GDMS is a typical solid analysis technique some attempts were made to analyze *solutions* as well [179]. Analyzing solutions can be performed by evaporation of a solution sample onto the surface of a conducting electrode by electrodepositing certain metals of the solution onto the cathode, by electrothermal vaporization (i.e. placing microliter aliquots of solution sample on a filament that serves as cathode, dry the sample to a residue film by passing currents through the filament, ash away organic constituents and finally atomize the residue in the glow discharge) and also by mixing a solution aliquot with powdered matrix material, followed by drying the mixture. Recently, a method was proposed for the direct analysis of aqueous solutions by GDMS [180]: the solution enters the vacuum of a glow discharge cell through a capillary and the water vapor itself is used as the discharge gas. This would be a low energy and cheap alternative (no noble gas) to ICP-MS.

Since stable glow discharge plasmas can be obtained with molecular gases (nitrogen, oxygen, air, water vapor, etc.), the glow discharge can also be used for *gas analysis*. McLuckey et al. designed a glow discharge ion source that used ambient air as discharge gas, to analyze trace impurities present in the sampled air [181]. A recent application is the detection of trace quantities of vapor explosives in the field by glow discharge ion trap mass spectrometry [157].

GDMS is mainly used for the analysis of inorganic samples, but some attempts were made to analyze *organic samples* as well. Three different introduction systems of the organic sample were reported in the literature, i.e.: (1) as liquid or gas chromatographic effluents [182]; (2) as deposits on the cathode surface [183]; and (3) directly as discharge gas components [157,181]. Some examples of organic samples that have recently been analyzed by GDMS, include the examination of polymers [176,184], the identification of impurities in petroleum [185] and the analysis of lead in waste oil samples [186].

Finally, in addition to the analysis of organic samples, another 'exotic' application of GDMS was reported in the literature, describing the analysis of materials of nuclear origin with the VG 9000 mass spectrometer placed in a glove-box [187]. More information about principles and applications of GDMS can be found in previous reviews [59,188,189].

3.3.2. Glow discharge optical emission spectrometry (GD-OES)

A long time before modern GDMS became popular, the glow discharge was already used both as line source and as direct analysis emission source [190,191], particularly in the hollow cathode configuration. However, for routine analysis of compacted metal samples, the breakthrough of GD-OES first occurred at the end of the 1960s with the work of

Grimm [126] who introduced the Grimm-type glow discharge (see above). Since then, the number of applications of GD-OES have been growing very rapidly.

The two sources that are now still extensively used in GD-OES are the hollow cathode lamp and the Grimm type source. Dispersive spectrometers with a diffraction grating are most frequently used for GD-OES. For sequential multielement determinations, monochromators in the Ebert or Czerny–Turner mountings are utilized, whereas simultaneous multielement analyses are performed with polychromators in the Paschen–Runge set-up [192]. However, multiplex spectrometers such as Hadamard transformation spectrometers [193] and especially Fourier transform interferometers [194] are also useful in combination with glow discharges. The radiation detection is mostly accomplished by photomultipliers. Glow discharges for OES operate at higher currents than for GDMS, i.e. 600–1000 V, 25–100 mA and 1–5 Torr for the Grimm source, and 200–500 V, 10–100 mA and 0.1–1 Torr for the hollow cathode lamp. Detection limits are in the order of 0.1–10 ppm.

The analytical applications of GD-OES are similar to the GDMS applications. Multielement analyses of bulk samples for major, minor and trace elements were described for most industrially important matrices, like steel and other metal alloys [195,196]. Moreover, the analysis of semiconductors by GD-OES was recently reported [197]. In addition, nonconductors can be analyzed with GD-OES, either by mixing with a conducting powder [198,199] or by using an RF glow discharge [130]. Some reports have also been made on the analysis of solution samples [198,200] and gas samples [201].

Finally, GD-OES is particularly widely applied in depth-profiling analyses. A large number of applications were reported [202–205]; among them are also some analyses performed with an RF powered glow discharge [137,203]. Most results are presented as relative intensity versus sputtering time and it is not straightforward to convert this into concentration of elements as a function of depth since the sputtering rate and the glow discharge conditions change during in-depth profiling of layers of varying chemical composition. Several empirically based quantification schemes were developed in the literature to deal with this problem [204,205]. For more information about GD-OES applications, the reader may consult other recent reviews [192,206,207].

3.3.3. Glow discharge atomic absorption and fluorescence spectrometry (GD-AAS and GD-AFS)

Both these techniques are less frequently used in glow discharge applications than GDMS and GD-OES, but they are receiving wider notice in the literature as their advantages come to be appreciated. Compared with GD-OES, for example, these methods have higher spectral resolution and suffer from fewer spectral interferences.

The use of a glow discharge as atomic absorption cell was first introduced by Russell and Walsh in 1959 [208] for the direct analysis of metals. Their observation that also atomic fluorescence was occurring in the cell eventually led to the use of GD-AFS as well [209]. During the 1960s and 1970s, several types of sputtering cells (i.e. hollow cathode cells and cells with flat electrodes) were investigated for use in GD-AAS and GD-AFS. In 1987, Bernhard [210] reported that gas jets striking the sputtering surface significantly increase the sampling rate and hence the absorption signal. A commercial atomic absorption cell, based on this principle and called 'Atomsource' [210] (Analyte Corp., Medford, OR), was made available and has further stimulated the applications of gas-jet-enhanced sputtering. In addition to DC sources, also an RF powered glow discharge device was recently introduced as atomization source for AAS [211].

As primary radiant sources for GD-AAS, modulated or pulsed hollow cathode lamps are commonly used. Tunable lasers are employed in special cases. Modulated Grimm-type cells are applied for multielement simultaneous GD-AAS because of the ease of changing the cathode to select the elements of interest. Hollow cathode lamps or tunable lasers are utilized as primary radiation sources for GD-AFS. Resulting from their high irradiances and narrow spectral bandwidths, the lasers yield detection limits that are many decades lower than those commonly obtained with GD-AAS and GD-AFS [146]. Even single atom detection was reported [212]. Typical discharge conditions for GD-AAS and GD-AFS are 4–10 Torr, 60–200 mA and 300–800 V.

As for GDMS and GD-OES, the applications of both GD-AAS and GD-AFS include the *bulk analysis*

of metals [213] and of a wide variety of *alloys* [209,214], the analysis of *powders* [215], *nonconductors* [216] and dried *solutions* [217]. Further information about basic principles and applications of GD-AAS and GD-AFS, can be found, for example in Ref. [218].

3.3.4. Glow discharges in a broader perspective

Beside the four analytical applications described previously, which make use of the glow discharge in its simple form as spectroscopic source, the glow discharge can also be employed in a hybrid construction, in combination with lasers, graphite furnaces, other discharges or magnetic fields. A brief overview of these application fields will be given here. Finally, some more exotic forms of glow discharges will be reported.

3.3.4.1. Laser-based methods. The development of cost-effective laser systems has generated a variety of laser techniques that can be coupled to a glow discharge. Since the atomization and the ionization/excitation steps occur independently from each other in the glow discharge, a laser can be employed to enhance either of these two steps.

First, the laser can be utilized to ablate material from the sample cathode, enhancing the atomization step [219]. This material ablation can also occur from a secondary sample (not the cathode) into the glow discharge [219,220]. In the latter case, the sample is not required to be conducting, expanding the analytical applications of glow discharges to the analysis of nonconductors without the need of applying RF power. Beside the enhanced atomization, the possibility of performing spatially resolved measurements is an additional advantage of this laser ablation method.

Second, the laser can also be used to enhance the excitation/ionization processes in the discharge. The usefulness of this laser enhancement was demonstrated in a variety of application areas such as atomic fluorescence (see before), optogalvanic effect spectroscopy [221,222] (i.e. the laser irradiation results in alterations in the ionization rate of the discharge, which are electrically detected by the resulting changes in voltage or current), laser enhanced ionization [222] (i.e. directly measuring the electrons released when the ionization in the discharge is enhanced due to laser photons) and resonance ionization mass spectrometry [219] (i.e. the laser is used for selective ionization enhancement of sputtered species in the discharge, increasing both the sensitivity and selectivity in GDMS). More information about these techniques is given in Ref. [223].

3.3.4.2. Furnace atomization nonthermal excitation spectrometry (FANES). As an analogy to the laser ablation glow discharge technique, FANES makes also use of an external atomization source (i.e. thermal vaporization from a graphite furnace) whereas the created atoms are excited and/or ionized in the glow discharge plasma. The concept of FANES was first proposed by Falk [224] who used a low-pressure DC glow discharge with the furnace playing the role of cathode (i.e. hollow cathode; HC-FANES). Another type of FANES system is based on a DC glow discharge in which the furnace comprises the anode (i.e. hollow anode; HA-FANES) [225]. The third type makes use of an RF glow discharge and is described by Blades and by Sturgeon and coworkers [226,227]. The latter sources also have a hollow anode geometry, but operate in helium at atmospheric pressure. These three types of sources are markedly different from classical glow discharge sources, i.e.: (1) sample volatilization is accomplished thermally and the rate of volatilization can be three orders of magnitude higher than typical sputtering rates; (2) all three FANES discharges involve 'hot' electrodes, with temperatures ranging from 800 K to 2800 K; and (3) the HA-FANES and RF-FANES operate at much higher pressures than conventional glow discharges, which results in a longer residence time for the analyte atoms in the plasma. More details can be found in Ref. [228].

3.3.4.3. Glow discharges enhanced by cross-excitation

In conventional glow discharges, the majority of the sputtered material is present as ground-state atoms. To increase the number densities of excited atoms and hence the emission line intensities and the sensitivity in GD-OES applications, a laser can be applied, as explained above, but also an auxiliary discharge can be employed, leading to cross-excitation or 'boosted' discharges. Several methods of cross-excitation have been investigated, i.e. the

application of: (1) a secondary DC discharge [229]; (2) an RF discharge [230]; and (3) a microwave discharge [198,230,231].

3.3.4.4. Magnetron discharges. Another method to improve the performance of a conventional glow discharge, is based on magnetic enhancement. One simple device among magnetically enhanced glow discharges is the magnetron glow discharge. In this device, permanent magnets are used to form a magnetic field of a few hundred Gauss in the plasma. Electrons in the plasma are forced to move in closed-loop trajectories parallel to the cathode surface. Hence, the electron path length is increased and the ionization of the discharge gas is significantly enhanced. Therefore, the magnetron discharge can operate at much lower pressures than conventional discharges. Lower pressure operation provides higher ion and electron kinetic energies, leading to higher atomization and excitation/ionization efficiencies and hence a better analytical sensitivity. However, while the sputtering in a conventional discharge is rather uniform, it is more or less confined to a ring in the magnetron. The characterization of magnetron discharges, both in DC and RF mode, and the applications in combination with mass spectrometry and atomic emission spectrometry are discussed, for example, in Refs [232–236].

3.3.4.5. Gas assisted sputtering glow discharges. Another way to increase the analytical sensitivity of a glow discharge is to use a gas-jet discharge. As a result of the gas jet impinging on the sample surface, the sputter-ablation is improved by both reduced redeposition and increased sample transport. This results in a higher sputtered atom population in the plasma and hence better analytical sensitivity. The gas-jet glow discharge was first developed by Bernhard in GD-AAS and has led to a commercially available GD-AAS source (see above). This type of glow discharge was also reported for other applications in AAS, OES and MS [237–239].

3.3.4.6. Elemental composition mapping of solid surfaces by glow discharges. A conventional glow discharge cannot be used for elemental mapping since the whole cathode is ablated at the same time and an average signal output is obtained. However, in a paper by Winchester and coworkers, an instrument is described which sustains a number of glow discharges simultaneously [240]. Each discharge exhibits atomic emission lines, characteristic of the sample surface beneath it. In this way, rapid macroscale (i.e. up to many tens of square centimeters) elemental composition mapping of solid surfaces can be performed, with a spatial resolution of about 1 mm.

3.3.4.7. A glow discharge using a solution as cathode

An exotic type of glow discharge in which an electrolyte solution is used as cathode and the anode is placed at a distance of a few millimeters from this solution was reported in the literature as forming the basis of glow discharge electrolysis [241]. Recently, such an arrangement has also been adapted as sputtering source in analytical chemistry [242]. A stable glow discharge was produced in atmospheric pressure air, using water as a cathode. By sputtering of the water cathode, the composition of water solutions could be analyzed by GD-OES.

3.3.4.8. Glow discharges used in technological applications

Although only glow discharge applications in analytical chemistry have been described up to now, it should be mentioned for the sake of completeness that glow discharges are even more extensively used in other application fields, ranging from the microelectronics industry (for plasma etching and modification of surfaces and for plasma vapor deposition of thin layers), to the plasma display panel technology (for television and computer screens), the laser business (sputtered metal ion hollow cathode lasers) and of course the lighting industry (e.g. neon lamps).

4. Conclusion

Glow discharge spectrometry is gaining increasing interest for the analysis of a variety of sample types, using mass spectrometry, optical emission spectrometry, atomic absorption and fluorescence spectrometry and also in hybrid constructions, with lasers, graphite furnaces, auxiliary discharges, magnetic fields, etc. For good results in all these application

fields, a clear insight in the fundamental glow discharge processes is desirable. Although the concept of a glow discharge seems to be quite simple, it is a rather complicated plasma, existing of a variety of plasma species, which can undergo a large number of different collision processes. By means of modeling on the one hand (i.e. simulation of the behavior of the plasma species) and plasma diagnostics on the other hand (i.e. measuring characteristic plasma properties), a better insight in the complexity and variety of plasma processes can be achieved.

Acknowledgements

A. Bogaerts is financially supported by the Flemish Fund for Scientific Research (FWO-Flanders). This research is also sponsored by the Federal Services of Scientific, Technical and Cultural Affairs (DWTC/SSTC) of the Prime Minister's Office through IUAP-IV (Conv. P/10).

References

[1] A. Bogaerts, R. Gijbels, Modeling of metastable argon atoms in a direct current glow discharge, Phys. Rev. A 52 (1995) 3743.

[2] R.J. Carman, A simulation of electron motion in the cathode sheath region of a glow discharge in argon, J. Phys. D 22 (1989) 55.

[3] H.A. Hyman, Electron impact ionization cross-sections for excited states of the rare gases (Ne, Ar, Kr, Xe), cadmium and mercury, Phys. Rev. A 20 (1979) 855.

[4] E. Eggarter, Comprehensive optical and collision data for radiation action II. Ar*, J. Chem. Phys. 62 (1975) 833.

[5] A.V. Phelps, Cross sections and swarm coefficients for nitrogen ions and neutrals in N_2 and argon ions and neutrals in Ar for energies from 0.1 eV to 10 keV, J. Chem. Phys. Ref. Data 20 (1991) 557.

[6] A. Bogaerts, R. Gijbels, The role of fast argon ions and atoms in the ionization of argon in a direct current glow discharge: a mathematical simulation, J. Appl. Phys. 78 (1995) 6427.

[7] C.M. Ferreira, A. Ricard, Modelling of the low-pressure argon positive column, J. Appl. Phys. 54 (1983) 2261.

[8] A.V. Phelps, The application of scattering cross sections to ion flux models in discharge sheaths, J. Appl. Phys. 76 (1994) 747.

[9] B. Chapman, Glow Discharge Processes, Wiley, New York, 1980.

[10] A. Bogaerts, R. Gijbels, J. Vlcek, Collisional–radiative model for an argon glow discharge, J. Appl. Phys. submitted.

[11] L. Vriens, Calculation of absolute ionisation cross sections of He, He*, He^+, Ne, Ne*, Ne^+, Ar, Ar*, Hg and Hg*, Phys. Lett. 8 (1964) 260.

[12] A.Z. Msezane, R.J.W. Henry, Electron impact excitation of atomic copper, Phys. Rev. A 33 (1986) 1631.

[13] L.A. Riseberg, W.F. Parks, L.D. Schearer, Penning ionization of Zn and Cd by noble gas metastable atoms, Phys. Rev. A 8 (1973) 1962.

[14] M. Bourène, J. Le Calve, De-excitation cross sections of metastable argon by various atoms and molecules, J. Chem. Phys. 58 (1973) 1452.

[15] S. Inaba, T. Goto, S. Hattori, Determination of the Penning excitation cross sections of Mg atoms by He, Ne and Ar metastable atoms, J. Phys. Soc. Jap. 52 (1983) 1164.

[16] J.W. Coburn, E. Kay, Plasma diagnostics of an RF-sputtering glow discharge, Appl. Phys. Lett. 18 (1971) 435.

[17] M.K. Levy, D. Serxner, A.D. Angstadt, R.L. Smith, K.R. Hess, Optical investigations of excitation processes responsible for ionized sputtered species in a low pressure, low current coaxial geometry glow discharge, Spectrochim. Acta B 46 (1991) 253.

[18] A. Bogaerts, R. Gijbels, Relative sensitivity factors in glow discharge mass spectrometry: the role of charge transfer ionization, J. Analyt. Atom. Spectrom. 11 (1996) 841.

[19] P.B. Farnsworth, J.P. Walters, Excitation processes in an RF-boosted, pulsed hollow cathode lamp, Spectrochim. Acta B 37 (1982) 773.

[20] E.B.M. Steers, R.J. Fielding, Charge transfer excitation processes in the Grimm lamp, J. Analyt. Atom. Spectrom. 2 (1987) 239.

[21] E.B.M. Steers, F. Leis, Excitation of the spectra of neutral and singly ionized atoms in the Grimm-type discharge lamp, with and without supplementary microwave excitation, Spectrochim. Acta B 46 (1991) 527.

[22] E.B.M. Steers, A.P. Thorne, Application of high-resolution fourier transform spectrometry to the study of glow discharge sources. Part 1. Excitation of iron and chromium spectra in a microwave boosted glow discharge source, J. Analyt. Atom. Spectrom. 8 (1993) 309.

[23] K. Wagatsuma, K. Hirokawa, Classification of singly ionized iron emission lines in the 160–250 nm wavelength region from Grimm-type glow discharge plasma, Spectrochim. Acta B 51 (1996) 349.

[24] R.S. Hudson, L.L. Skrumeda, W.J. Whaling, Fe II level populations in a hollow cathode discharge, J. Quant. Spectrosc. Radiat. Transfer 38 (1987) 1.

[25] P. Baltayan, J.C. Pebay-Peyroula, N. Sadeghi, Determination of the rate constants for population of the individual Cd^{+}* levels in thermal Penning and charge transfer reactions of He^+ (2^3S_1) and He^+ with cadmium, J. Phys. B 18 (1985) 3618.

[26] P. Baltayan, J.C. Pebay-Peyroula, N. Sadeghi, Excitation of Zn^{+}* levels in Penning and charge transfer reactions of He* (2^3S_1) and He^+ with zinc, J. Phys. B 19 (1986) 2695.

[27] A.K. Belyaev, Charge exchange with ion excitation in collisions of helium ions with mercury atoms, J. Phys. B 26 (1993) 3877.

[28] H.A. Schuessler, C.H.Holder Jr., O. Chun-Sing, Orbiting

charge transfer cross sections between He^+ ions and cesium atoms at near-thermal ion–atom energies, Phys. Rev. A 28 (1983) 1817.
[29] D. Fogel, Y.A. Tolmachev, Nonresonant charge transfer of $He^+ + Rb$ at thermal energies, Opt. Spectrosc. 49 (1980) 450.
[30] V.A. Kartazaev, Y.A. Piotrovskii, Y.A. Tolmachev, Charge exchange and Penning ionization in a pulsed discharge in a mixture of neon and zinc, Opt. Spectrosc. 44 (1978) 362.
[31] S.C. Rae, R.C. Tobin, Sputtering in the presence of a rapid gas flow, J. Appl. Phys. 64 (1988) 1418.
[32] K.B. Butterfield, D.C. Gerstenberger, T. Shay, W.L. Little, G.J. Collins, Collisional quenching of Xe^+ (^2p) and He 2^3S metastables by calcium and strontium metal vapors, J. Appl. Phys. 49 (1978) 3088.
[33] E.M. van Veldhuizen, F.J. de Hoog, Analysis of a Cu–Ne hollow cathode glow discharge at intermediate currents, J. Phys. D 17 (1984) 953.
[34] K. Danzmann, M. Kock, Population densities in a titanium hollow cathode, J. Phys. B 14 (1981) 2989.
[35] L. Csillag, M. Janossy, K. Rozsa, T. Salamon, Near infrared CW laser oscillation in Cu II, Phys. Lett. A 50 (1974) 13.
[36] A. Bogaerts, R. Gijbels, W.J. Goedheer, Hybrid Monte Carlo–fluid model of a direct current glow discharge, J. Appl. Phys. 78 (1995) 2233.
[37] A. Bogaerts, R. Gijbels, W.J. Goedheer, Two-dimensional model of a direct current glow discharge: description of the electrons, argon ions and fast argon atoms, Analyt. Chem. 68 (1996) 2296.
[38] A. Bogaerts, R. Gijbels, Role of sputtered Cu atoms and ions in a direct current glow discharge: combined fluid and Monte Carlo model, J. Appl. Phys. 79 (1996) 1279.
[39] A. Bogaerts, R. Gijbels, Two-dimensional model of a direct current glow discharge: description of the argon metastable atoms, sputtered atoms and ions, Analyt. Chem. 68 (1996) 2676.
[40] E.W. McDaniel, J.B.A. Mitchell, M.E. Rudd, Atomic Collisions: Heavy Particle Projectiles, Wiley, New York, 1993.
[41] H.S.W. Massey, E.H.S. Burhop, Electronic and Ionic Impact Phenomena, Oxford University Press, Oxford, 1952.
[42] V.S. Vorob'ev, Kinetics of ionization and recombination in low-temperature plasmas, Plasma Sources Sci. Technol. 4 (1995) 163.
[43] M.A. Biondi, Studies of the mechanism of electron-ion recombination I., Phys. Rev. 129 (1963) 1181.
[44] R.F. Stebbings, Gaseous and surface reactions involving helium metastable atoms and resonance photons, Proc. Roy. Soc. Lond. A 241 (1957) 270.
[45] J.B. Hasted, Collisions of metastable atoms, J. Appl. Phys. 30 (1959) 22.
[46] H. Oechsner, Electron yields from clean polycrystalline metal surfaces by noble-gas-ion bombardment at energies around 1 keV, Phys. Rev. B 17 (1978) 1052.
[47] A.V. Phelps, private communication.
[48] W.W. Harrison, B.L. Bentz, Glow discharge mass spectrometry, Prog. Analyt. Spectrosc. 11 (1988) 53.
[49] R.V. Stuart, G.K. Wehner, Energy distribution of sputtered Cu atoms, J. Appl. Phys. 35 (1964) 1819.
[50] P. Sigmund, Theory of sputtering. I. Sputtering yield of amorphous and polycrystalline targets, Phys. Rev. 184 (1969) 383.
[51] Y. Yamamura, N. Matsunami, N. Itoh, Theoretical studies on an empirical formula for sputtering yield at normal incidence, Radiat. Effic. 71 (1983) 65.
[52] N. Matsunami, Y. Yamamura, Y. Itikawa, N. Itoh, Y. Kazumata, S. Miyagawa, K. Morita, R. Shimizu, H. Tawara, Energy dependence of the ion-induced sputtering yields of monoatomic solids, Atom. Data Nucl. Data Tables 31 (1984) 1.
[53] M.T. Robinson, I.M. Torrens, Computer simulation of atomic displacement cascades in solids in the binary collision approximation, Phys. Rev. B 9 (1974) 5008.
[54] H.A. Oechsner, Sputtering—review of some experimental and theoretical aspects, Appl. Phys. 8 (1975) 185.
[55] A. Benninghoven, F.G. Rüdenauer, H.W. Werner, Secondary Ion Mass Spectrometry: Basic Concepts, Instrumental Aspects, Applications and Trends, Wiley, New York, 1987.
[56] E. W. McDaniel, Collision Phenomena in Ionized Gases, Wiley, New York, 1964.
[57] G. Francis, The glow discharge at low pressure, in: S. Flügge (Ed.), Handbuch der Physik, vol. 22, Springer, Berlin, 1956.
[58] D.B. Graves, K.F. Jensen, A continuum model of DC and RF discharges, IEEE Trans. Plasma Sci. PS-14 (1986) 78.
[59] J.P. Boeuf, A two-dimensional model of DC glow discharges, J. Appl. Phys. 63 (1988) 1342.
[60] M. Meyyappan, T.R. Govindan, Radio frequency discharge modeling: moment equations approach, J. Appl. Phys. 74 (1993) 2250.
[61] J.D.P. Passchier, W.J. Goedheer, Relaxation phenomena after laser-induced photodetachment in electronegative RF discharges, J. Appl. Phys. 73 (1993) 1073.
[62] J.D.P. Passchier, W.J. Goedheer, A two-dimensional fluid model for an argon RF discharge, J. Appl. Phys. 74 (1993) 3744.
[63] I. Abril, Alacant: modeling of glow discharge sputtering systems, Comput. Phys. Commun. 51 (1988) 413.
[64] J.P. Boeuf, E. Marode, A Monte Carlo analysis of an electron swarm in a non-uniform field: the cathode region of a glow discharge in helium, J. Phys. D 15 (1982) 2169.
[65] M.J. Kushner, Mechanisms for power deposition in Ar/SiH_4 capacitively coupled rf discharges, IEEE Trans. Plasma Sci. 14 (1986) 188.
[66] Z. Donko, K. Rozsa, R.C. Tobin, Monte Carlo analysis of the electrons' motion in a segmented hollow cathode discharge, J. Phys. D 29 (1996) 105.
[67] M. Surendra, D.B. Graves, G.M. Jellum, Self-consistent model of a direct current glow discharge: treatment of fast electrons, Phys. Rev. A 41 (1990) 1112.
[68] J.-P. Boeuf, L.C. Pitchford, Pseudospark discharges via computer simulation, IEEE Trans. Plasma Sci. PS-19 (1991) 286.
[69] A. Fiala, L.C. Pitchford, J.P. Boeuf, Two-dimensional, hybrid model of low-pressure glow discharges, Phys. Rev. E 49 (1994) 5607.
[70] A. Bogaerts, M. van Straaten, R. Gijbels, Monte Carlo simulation of an analytical glow discharge: motion of electrons, ions and fast neutrals in the cathode dark space, Spectrochim. Acta B 50 (1995) 179.

[71] A. Bogaerts, M. van Straaten, R. Gijbels, Description of the thermalization process of the sputtered atoms in a glow discharge, using a three-dimensional Monte Carlo method, J. Appl. Phys. 77 (1995) 1868.
[72] A. Bogaerts, R. Gijbels, Mathematical description of a direct current glow discharge in argon, Fresenius' J. Analyt. Chem. 355 (1996) 853.
[73] A. Bogaerts, Mathematical modeling of a direct current glow discharge in argon, Ph.D. Dissertation, University of Antwerp, 1996.
[74] A. Bogaerts, R. Gijbels, Computer simulation of an analytical direct current glow discharge in argon: influence of the cell dimensions on the plasma quantities, J. Analyt. Atom. Spectrom. 12 (1997) 751.
[75] A. Bogaerts, R. Gijbels, Modeling of glow discharge sources with flat and pin cathodes and implications for mass spectrometric analysis, J. Am. Soc. Mass Spectrom. 8 (1997) 1021.
[76] F.W. Aston, Experiments on the length of the cathode dark space with varying current densities and pressures in different gases, Proc. Roy. Soc. Lond. Ser. A 79 (1907) 80.
[77] A. Bogaerts, R.D. Guenard, B.W. Smith, J.D. Winefordner, W.W. Harrison, R. Gijbels, Three-dimensional density profiles of the argon metastable atoms in a direct current glow discharge: experimental study and comparison with calculations, Spectrochim. Acta B 52 (1997) 219.
[78] A. Bogaerts, E. Wagner, B.W. Smith, J.D. Winefordner, D. Pollmann, W.W. Harrison, R. Gijbels, Three-dimensional density profiles of sputtered atoms and ions in a direct current glow discharge: experimental study and comparison with calculations, Spectrochim. Acta B 52 (1997) 205.
[79] M. van Straaten, A. Bogaerts, R. Gijbels, Experimental determination of energy distributions of ions bombarding the cathode surface in a glow discharge, Spectrochim. Acta B 50 (1995) 583.
[80] A. Bogaerts, R. Gijbels, Calculation of crater profiles on a flat cathode in a direct current glow discharge and comparison with experiment, Spectrochim. Acta B 52 (1997) 765.
[81] C. Jonkers, Analyse van metalen en metaaloppervlakken met glimontladingsmassaspectrometrie, Ph.D. Dissertation, University of Antwerp, 1995.
[82] E. Dwight, B.W. Billings, D.F. Bleil, R.K. Cook, H.M. Crosswhite, H.P.R. Frederikse, R.B. Lindsay, J.B. Marion, M.W. Zemansky, American Institute of Physics Handbook, McGraw-Hill, New York, 1972.
[83] W. Vieth, J.C. Huneke, Relative sensitivity factors in glow discharge mass spectrometry, Spectrochim. Acta B 46 (1991) 137.
[84] A. Bogaerts, R. Gijbels, Comprehensive description of a Grimm-type glow discharge source used for optical emission spectrometry: a mathematical simulation, Spectrochim. Acta B in press.
[85] A. Bogaerts, R. Gijbels, Comparison of argon and neon as discharge gases in a direct current glow discharge: a mathematical simulation, Spectrochim. Acta B 52 (1997) 553.
[86] A. Vertes, R. Gijbels, F. Adams, Diagnostics and modeling of plasma processes in ion sources, Mass Spectrom. Rev. 9 (1990) 71.
[87] I. Langmuir, H. Mott-Smith, Studies of electric discharges in gases at low pressures, Part I–V, General Electric Review, XXVII, nos 7, 8, 9, 11, 12 (1924).
[88] D. Fang, R.K. Marcus, Use of a cylindrical Langmuir probe for the characterization of charged particle populations in a planar, diode glow discharge device, Spectrochim. Acta B 45 (1990) 1053.
[89] I.D. Sudit, R.C. Woods, A workstation based Langmuir probe system for low-pressure DC plasmas, Rev. Sci. Instrum. 64 (1993) 2440.
[90] A. Bogaerts, A. Quentmeier, N. Jakubowski, R. Gijbels, Plasma diagnostics of analytical glow discharges in argon and in neon: Langmuir probe and optical emission spectrometry measurements, Spectrochim. Acta B 50 (1995) 1337.
[91] Y. Ye, R.K. Marcus, Application of a tuned Langmuir probe for the diagnostic study of radio frequency glow discharges: instrumentation and theory, Spectrochim. Acta B 50 (1995) 997.
[92] M.J. Heintz, G.M. Hieftje, Langmuir probe measurements of a pulsed and steady-state RF glow discharge source and of an RF planar magnetron source, Spectrochim. Acta B 51 (1996) 1629.
[93] Y. Ye, R.K. Marcus, Effects of limiting orifice (anode) geometries on charged particle characteristics in an analytical radio frequency glow discharge as determined by Langmuir, current and voltage probes, J. Analyt. Atom. Spectrom. 12 (1997) 33.
[94] P.A. Buger, S. El. Alfy, Messung von Anregungstemperaturen in einer Glimmentladingslampe, Z. Naturforsch. 30a (1975) 466.
[95] D.M. Mehs, T.M. Niemczyk, Excitation temperatures in the hollow cathode discharge, Appl. Spectrosc. 35 (1981) 66.
[96] M. Kubota, Y. Fujishiro, R. Ishida, Selection of spectral lines and transition probability data in plasma temperature measurements by photoelectric scanning spectrometry, Spectrochim. Acta B 36 (1981) 697.
[97] M. Kuraica, N. Konjevic, M. Platisa, D. Pantelic, Plasma diagnostics of the Grimm-type glow discharge, Spectrochim. Acta B 47 (1992) 1173.
[98] S.K. Ohordnik, W.W. Harrison, Plasma diagnostic measurements in the cryogenically cooled glow discharge, J. Analyt. Atom. Spectrom. 9 (1994) 991.
[99] P.E. Walters, T.L. Chester, J.D. Winefordner, Measurement of excitation, ionization and electron temperatures and positive ion concentrations in a 144 MHz inductively coupled radio frequency plasma, Appl. Spectrosc. 31 (1977) 1.
[100] N.P. Ferreira, H.G.C. Human, L.R.P. Butler, Kinetic temperatures and electron densities in the plasma of a side-view Grimm-type glow discharge, Spectrochim. Acta B 35 (1980) 287.
[101] Z.M. Jelenak, Z.B. Velikic, J.V. Bozin, Z.L. Petrovic, B.M. Jelenkovic, Electronic excitation of the 750 and 811 nm lines of argon, Phys. Rev. E 47 (1993) 3566.
[102] E.W. Eckstein, J.W. Coburn, E. Kay, Diagnostics of an RF sputtering glow discharge-correlation between atomic absorption and mass spectrometry, Int. J. Mass Spectrom. Ion Physics 17 (1975) 129.

[103] K.R. Hess, W.W. Harrison, The role of metastable atoms in glow discharge ionization processes, Analyt. Chem. 60 (1988) 691.
[104] M. Tuszewski, A compact mass spectrometer for plasma discharge ion analysis, Rev. Sci. Instrum. 67 (1996) 2215.
[105] R.-C. Deng, P. Williams, Suppresion of cluster ion interferences in glow discharge mass spectrometry by sampling high-energy ions from a reversed hollow cathode ion source, Analyt. Chem. 66 (1994) 1890.
[106] B.E. Thompson, K.D. Allen, A.D. Richards, H.H. Sawin, Ion bombardment energy distributions in radio-frequency glow discharge systems, J. Appl. Phys. 59 (1986) 1890.
[107] W.M. Greene, M.A. Hartney, W.G. Oldham, D.W. Hess, Ion transit through capacitively coupled Ar sheaths: ion current and energy distribution, J. Appl. Phys. 63 (1988) 1367.
[108] S. Kumar, P.K. Ghosh, Ion kinetic energy distribution in nitrogen DC discharge, Int. J. Mass Spectrom. Ion Process. 127 (1993) 105.
[109] J.K. Olthoff, R.J. Van Brunt, S.B. Radovanov, Ion kinetic energy distributions in argon RF glow discharges, J. Appl. Phys. 72 (1992) 4566.
[110] J.K. Olthoff, R.J. Van Brunt, S.B. Radovanov, J.A. Rees, R. Surowiec, Kinetic energy distributions of ions sampled from argon plasmas in a parallel-plate, radio frequency reference cell, J. Appl. Phys. 75 (1994) 115.
[111] K.-U. Riemann, U. Ehlemann, K. Wiesemann, The ion energy distribution in front of a negative wall, J. Phys. D 25 (1992) 620.
[112] U. Kortshagen, M. Zethoff, Ion energy distribution functions in a planar inductively coupled RF discharge, Plasma Sources Sci. Technol. 4 (1995) 541.
[113] P. Gill, C.E. Webb, Electron energy distributions in the negative glow and their relevance to hollow cathode lasers, J. Phys. D 10 (1977) 299.
[114] N.P. Ferreira, J.A. Strauss, H.G.C. Human, Distribution of metastable argon atoms in the modified Grimm-type electrical discharge, Spectrochim. Acta B 37 (1982) 273.
[115] N.P. Ferreira, H.G.C. Human, A study of the density of sputtered atoms in the plasma of the modified Grimm-type glow discharge source, Spectrochim. Acta B 36 (1981) 215.
[116] N.I. Uzelac, F. Leis, Measurement of gas temperatures and metastable state densities in a microwave boosted glow discharge using a diode laser, Spectrochim. Acta B 47 (1992) 877.
[117] A.J. Langley, R.A. Beaman, A.N. Davies, W.J. Jones, J. Baran, Concentration-modulated absorption spectroscopy. I., Chem. Phys. 101 (1986) 117.
[118] R.M. Allott, M. Kubinyl, A. Grofcsik, W.J. Jones, R.S. Mason, Temporal and spatial distribution profiles of lithium atoms in low-pressure discharges by concentration-modulated absorption spectroscopy, J. Chem. Soc. Faraday Trans. 91 (1995) 1297.
[119] G.M. Hieftje, Plasma diagnostic techniques for understanding and control, Spectrochim. Acta B 47 (1992) 3.
[120] N.N. Sesi, D.S. Hanselman, P. Galley, J. Homer, M. Huang, G.M. Hieftje, An imaging based instrument for fundamental plasma studies, Spectrochim. Acta B 52 (1997) 83.
[121] D.M. Manos, J.L. Cecchi, C.W. Cheah, H.F. Dylla, Diagnostics of low temperature, plasmas: the electron component, Thin Solid Films 195 (1991) 319.
[122] M. Fadlallah, J.-P. Booth, J. Derouard, N. Sadeghi, Sheath electric field oscillation and ion kinetics in radio frequency discharges, J. Appl. Phys. 79 (1996) 8976.
[123] I.R. Videnovic, N. Konjevic, M.M. Kuraica, Spectroscopic investigations of a cathode fall region of the Grimm-type glow discharge, Spectrochim. Acta B 51 (1996) 1707.
[124] J.P. Booth, J. Derouard, M. Fadlallah, L. Cabaret, J. Pinard, Electric field measurements in discharges by Doppler-free two-photon laser Stark spectroscopy of atomic hydrogen, Opt. Commun. 132 (1996) 363.
[125] M.M. Kuraica, N. Konjevic, I.R. Videnovic, Spectroscopic study of the cathode fall region of Grimm-type glow discharge in helium, Spectrochim. Acta B 52 (1997) 745.
[126] W. Grimm, Eine neue Glimmentladungslampe für die optische Emissionsspektralanalyse, Spectrochim. Acta B 23 (1968) 443.
[127] J.W. Coburn, E. Kay, A new technique for the elemental analysis of thin surface layers of solids, Appl. Phys. Lett. 19 (1971) 350.
[128] D.L. Donohue, W.W. Harrison, Radiofrequency cavity ion source in solids mass spectrometry, Analyt. Chem. 47 (1975) 1528.
[129] D.C. Duckworth, R.K. Marcus, Radiofrequency powered glow discharge atomization/ionization source for solids mass spectrometry, Analyt. Chem. 61 (1989) 1879.
[130] M.R. Winchester, R.K. Marcus, Applicability of a radiofrequency powered glow discharge for the direct solids analysis of non-conducting materials by atomic emission spectrometry, J. Analyt. Atom. Spectrom. 5 (1990) 575.
[131] R.K. Marcus, P.R. Cable, D.C. Duckworth, M.V. Buchanan, J.M. Pochkowski, R.R. Weller, A simple, lensless interface of an RF glow discharge device to an FT-ICR (FTMS), Appl. Spectrosc. 46 (1992) 1327.
[132] S.A. McLuckey, G.L. Glish, D.C. Duckworth, R.K. Marcus, Radio frequency glow discharge ion trap mass spectrometry, Analyt. Chem. 64 (1992) 1606.
[133] C.R.Shick Jr., A. Raith, R.K. Marcus, Complementary radiofrequency glow discharge source for a commercial quadrupole mass spectrometer system, J. Analyt. Atom. Spectrom. 8 (1993) 1043.
[134] D.C. Duckworth, D.L. Donohue, D.J. Smith, T.A. Lewis, R.K. Marcus, Design and characterization of a radiofrequency powered glow discharge source for double focusing mass spectrometers, Analyt. Chem. 65 (1993) 2478.
[135] T.R. Harville, R.K. Marcus, Line selection and evaluation of radiofrequency glow discharge atomic emission spectrometry for the analysis of copper and aluminum alloys, Analyt. Chem. 65 (1993) 3636.
[136] D.P. Myers, M.J. Heintz, P.P. Mahoney, G. Li, G.M. Hieftje, Characterization of a radiofrequency glow discharge/time-of-flight mass spectrometer, Appl. Spectrosc. 48 (1994) 1337.
[137] N. Bordel-Garcia, R. Pereiro-Garcia, M. Fernandez-Garcia, A. Sanz-Medel, T.R. Harville, R.K. Marcus, Preliminary study of the role of discharge conditions on the in-depth

analysis of conducting thin films by radio frequency glow discharge optical emission spectrometry, J. Analyt. Atom. Spectrom. 10 (1995) 671.
[138] A.I. Saprykin, J.S. Becker, H.-J. Dietze, Characterization and optimization of a radio frequency glow discharge ion source for a high resolution mass spectrometer, J. Analyt. Atom. Spectrom. 10 (1995) 897.
[139] S. De Gendt, R. Van Grieken, S.K. Ohorodnik, W.W. Harrison, Parameter evaluation for the analysis of oxide-based samples with radio frequency glow discharge mass spectrometry, Analyt. Chem. 67 (1995) 1026.
[140] M.J. Heintz, G.M. Hieftje, Effect of driving frequency on the operation of a radiofrequency glow discharge emission source, Spectrochim. Acta B 50 (1995) 1125.
[141] C.R.Shick Jr, , R.K. Marcus, Optimization of discharge parameters for a flat-type radiofrequency glow discharge source coupled to a quadrupole mass spectrometer system, Appl. Spectrosc. 50 (1996) 454.
[142] V. Hoffmann, H.-J. Uhlemann, F. Präßler, K. Wetzig, D. Birus, New hardware for radiofrequency powered glow discharge spectroscopies and its capabilities for analytical applications, Fresenius' J. Analyt. Chem. 355 (1996) 826.
[143] J.A. Klingler, C.M. Barshick, W.W. Harrison, Factors influencing ion signal profiles in pulsed glow discharge mass spectrometry, Analyt. Chem. 63 (1991) 2571.
[144] J.A. Klingler, W.W. Harrison, Glow discharge mass spectrometry using pulsed dual cathodes, Analyt. Chem. 63 (1991) 2982.
[145] M.R. Winchester, R.K. Marcus, Emission characteristics of a pulsed, radiofrequency glow discharge atomic emission device, Analyt. Chem. 64 (1992) 2067.
[146] M. Glick, B.W. Smith, J.D. Winefordner, Laser excited atomic fluorescence in a pulsed hollow cathode glow discharge, Analyt. Chem. 62 (1990) 157.
[147] W. Hang, W.O. Walden, W.W. Harrison, Microsecond pulsed glow discharge as an analytical spectroscopic source, Analyt. Chem. 68 (1996) 1148.
[148] W. Hang, C. Baker, B.W. Smith, J.D. Winefordner, W.W. Harrison, Microsecond-pulsed glow discharge time-of-flight mass spectrometry: analytical advantages, J. Analyt. Atom. Spectrom. 12 (1997) 143.
[149] F.W. Aston, Mass Spectra and Isotopes, 2nd ed., Longmans, Green and Co, New York, 1942.
[150] K.T. Bainbridge, E.B. Jordon, Mass spectrum analysis. 1. The mass spectrograph, 2. The existence of isobars of adjacent elements, Phys. Rev. 50 (1936) 282.
[151] W.W. Harrison, C.W. Magee, Hollow cathode ion source for solids mass spectrometry, Analyt. Chem. 46 (1974) 461.
[152] C.G. Bruhn, B.L. Bentz, W.W. Harrison, Simplified solids mass spectrometry combining a glow discharge source with a quadrupole mass filter, Analyt. Chem. 50 (1978) 373.
[153] R.K. Marcus, W.W. Harrison, The hollow cathode plume: A plasma emission source for solids, Spectrochim. Acta B 40 (1985) 933.
[154] J.E. Cantle, E.F. Hall, C.J. Shaw, P.J. Turner, A plasma discharge source mass spectrometer for inorganic analysis, Int. J. Mass Spectrom. Ion Process. 46 (1983) 11.
[155] N. Jakubowski, D. Stüwer, G. Tölg, Improvement of ion source performance in glow discharge mass spectrometry, Int. J. Mass Spectrom. Ion Process. 71 (1986) 183.
[156] R.C. Hutton, A. Raith, Analysis of pure metals using a quadrupole-based glow discharge mass spectrometer. Part 1. Analysis of copper, J. Analyt. Atom. Spectrom. 7 (1992) 623.
[157] S.A. McLuckey, D.E. Goeringer, K.G. Asano, G. Vaidyanathan, J.L. Stephenson Jr., High explosives vapor detection by glow discharge–ion trap mass spectrometry, Rapid. Commun. Mass Spectrom. 10 (1996) 287.
[158] F.L. King, W. W, Harrison, Collision-induced dissociation of polyatomic ions in glow discharge mass spectrometry, Int. J. Mass. Spectrom. Ion Process. 89 (1989) 171.
[159] C.H. Watson, C.M. Barshick, J. Wronka, F.H. Laukien, J.R. Eyler, Pulsed-gas glow discharge for ultrahigh mass resolution measurements with fourier transform ion cyclotron resonance mass spectrometry, Analyt. Chem. 68 (1996) 573.
[160] A.P. Mykytiuk, P. Semeniuk, S. Berman, Analysis of high purity metals and semiconductor materials by glow discharge mass spectrometry, Spectrochim. Acta Rev. 13 (1990) 1.
[161] K. Robinson, E.F.H. Hall, Glow discharge mass spectrometry for nuclear materials, J. Metals 39 (1987) 14.
[162] N.E. Sanderson, E. Hall, J. Clark, P. Charalambous, D. Hall, Glow discharge mass spectrometry—a powerful technique for the elemental analysis of solids, Mikrochim. Acta 1 (1987) 275.
[163] N. Jakubowski, I. Feldmann, D. Stüwer, Comparison of ICP-MS with spark ablation and GDMS for direct element analysis of conductive solids, Spectrochim. Acta B 50 (1995) 639.
[164] L.R. Riciputi, D.C. Duckworth, C.M. Barshick, D.H. Smith, Isotope ratio measurements using glow discharge mass spectrometry, Int. J. Mass Spectrom. Ion Process. 146/147 (1995) 55.
[165] K.L. Goodner, J.R. Eyler, C.M. Barshick, D.H. Smith, Elemental quantification based on argides, dimers and doubly charged glow discharge ions, Int. J. Mass Spectrom. Ion Process. 146/147 (1995) 65.
[166] R.W. Smithwick III, D.W. Lynch, J.C. Franklin, Relative ion yields measured with a high resolution glow discharge mass spectrometer operated with an argon/hydrogen mixture, J. Am. Soc. Mass Spectrom. 4 (1993) 278.
[167] G.I. Ramendik, D.A. Tyurin, Yu.I. Babikov, Is a universal model for ion formation during mass spectrometric elemental analysis possible?, Analyt. Chem. 62 (1990) 2501.
[168] S.L. Tong, W.W. Harrison, Glow discharge mass spectrometric analysis of nonconducting materials, Spectrochim. Acta B 48 (1993) 1237.
[169] S. De Gendt, W. Schelles, R. Van Grieken, V. Müller, Quantitative analysis of iron-rich and other oxide-based samples by means of glow discharge mass spectrometry, J. Analyt. Atom. Spectrom. 10 (1995) 681.
[170] D.M.P. Milton, R.C. Hutton, Investigations into the suitability of using a secondary cathode to analyse glass using glow discharge mass spectrometry, Spectrochim. Acta B 48 (1993) 39.
[171] W. Schelles, S. De Gendt, V. Müller, R. Van Grieken,

Evaluation of secondary cathodes for glow discharge mass spectrometry analysis of different nonconducting sample types, Appl. Spectrosc. 49 (1995) 939.
[172] W. Schelles, K. Maes, S. De Gendt, R. Van Grieken, Glow discharge mass spectrometric analysis of atmospheric particulate matter, Analyt. Chem. 68 (1996) 1136.
[173] W. Schelles, R. Van Grieken, Direct current glow discharge mass spectrometric analysis of macor ceramics using a secondary cathode, Analyt. Chem. 68 (1996) 3570.
[174] W. Schelles, S. De Gendt, R. Van Grieken, Optimization of secondary cathode thickness for direct current glow discharge mass spectrometric analysis of glass, J. Analyt. At. Spectrom. 11 (1996) 937.
[175] M. Betti, S. Giannarelli, T. Hiernaut, G. Rasmussen, L. Koch, Detection of trace radioisotopes in soil, sediment and vegetation by glow discharge mass spectrometry, Fresenius' J. Analyt. Chem. 355 (1996) 642.
[176] W. Schelles, R. Van Gricken, Direct current glow discharge mass spectrometry for elemental characterization of polymers, Analyt. Chem. 69 (1997) 2931.
[177] N. Jakubowski, D. Stüwer, Application of glow discharge mass spectrometry with low mass resolution for in-depth analysis of technical surface layers, J. Analyt. Atom. Spectrom. 7 (1992) 951.
[178] A. Raith, R.C. Hutton, J.C. Huneke, Optimization of quantitative depth profiling with glow discharge mass spectrometry. Part 1. Optimization studies on crater shape and time-depth conversion, J. Analyt. Atom. Spectrom. 8 (1993) 867.
[179] N. Jakubowski, D. Stüwer, G. Tölg, Microchemical determination of platinum and iridium by glow discharge mass spectrometry, Spectrochim. Acta 46B (1991) 155.
[180] G.G. Sikharudlidze, Glow discharge plasma sources for liquids, poster presented at the 1996 Winter Conference on Plasma Spectrochemistry, Fort Lauderdale, FL, 1996.
[181] S.A. McLuckey, G.L. Glish, K.G. Asano, B.G. Grant, Atmospheric sampling glow discharge ionization source for the determination of trace organic compounds in ambient air, Analyt. Chem. 60 (1988) 2220.
[182] D. Carazatto, M.J. Bertrand, Characterization of a glow discharge ion source for the mass spectrometric analysis of organic compounds, J. Am. Soc. Mass Spectrom. 5 (1994) 305.
[183] R. Mason, D. Milton, Glow discharge mass spectrometry of some organic compounds, Int. J. Mass Spectrom. Ion Process. 91 (1989) 209.
[184] R.K. Marcus, T.R. Harville, Y. Mei, C.R. Shick Jr., Rf-powered glow discharges: elemental analysis across the solids spectrum, Analyt. Chem. 66 (1994) 902A.
[185] C.M. Barshick, D.H. Smith, J.H. Hackney, B.A. Cole, J.A. Cole, J.W. Wade, Glow discharge mass spectrometric analysis of trace metals in petroleum, Analyt. Chem. 66 (1994) 730.
[186] C.M. Barshick, D.H. Smith, J.W. Wade, C.K. Bayne, Isotope dilution glow discharge mass spectrometry as applied to the analysis of lead in waste oil samples, J. Analyt. Atom. Spectrom. 9 (1994) 83.
[187] M. Betti, G. Rasmussen, T. Hiernaut, L. Koch, D.M.P. Milton, R.C. Hutton, Adaptation of a glow discharge mass spectrometer in a glove-box for the analysis of nuclear materials, J. Analyt. Atom. Spectrom. 9 (1994) 385.
[188] W.W. Harrison, Glow discharge mass spectrometry, in: F. Adams, R. Gijbels, R. Van Grieken (Eds), Inorganic Mass Spectrometry, Wiley, New York, 1988.
[189] F.L. King, W.W. Harrison, Glow discharge mass spectrometry, in: R.K. Marcus (Ed.), Glow Discharge Spectroscopies, Plenum Press, New York, 1993.
[190] H. Schüler and A. Michel, Über zwei neue hohlkathoden-Entladungsröhren, Spectrochim. Acta 5 (1952) 322.
[191] W.W. Harrison, N.J. Prakash, Trace element analysis of solutions by hollow cathode excitation, Analyt. Chim. Acta 49 (1970) 151.
[192] J.A.C. Broekaert, Atomic emission spectrometry, in: R.K. Marcus (Ed.), Glow Discharge Spectroscopies, Plenum Press, New York, 1993.
[193] P.J. Treado, M.D. Morris, A thousand points of light: the Hadamard transform in chemical analysis and instrumentation, Analyt. Chem. 61 (1989) 723A.
[194] J.A.C. Broekaert, K.R. Brushwyler, C.A. Monnig, G.M. Hieftje, Fourier transform atomic emission spectrometry with a Grimm-type glow discharge source, Spectrochim. Acta B 45 (1990) 769.
[195] M. Dogan, Spektrochemische Bestimmung der Hauptbestandteile von Cu-Al-Binärlegierungen mit der Glimmentladungslampe als Lichtquelle, Spectrochim. Acta B 36 (1981) 103.
[196] K. Wagatsuma, K. Hirokawa, Analysis of iron-base alloys by low wattage glow discharge emission spectrometry, Analyt. Chem. 56 (1984) 908.
[197] I.M. Dharmadasa, M. Yves, J.S. Brooks, G.H. France, S.J. Brown, Application of glow discharge optical emission spectroscopy to study semiconductors and semiconductor devices, Semicond. Sci. Technol. 10 (1995) 369.
[198] S. Caroli, O. Senofonte, M.G. Del Monte Tamba, M. Cilia, I.B. Brenner, M. Dvorochek, The analysis of non-conducting materials by low pressure discharges: sediments and dry residues, Spectrochim. Acta B 48 (1993) 877.
[199] F. Flórian, W. Fischer, H. Nickel, Direct solid sample analysis of silicon carbide powders by direct current glow discharge and direct current arc emission spectrometry, J. Analyt. Atom. Spectrom. 9 (1994) 257.
[200] C.M. Strange, R.K. Marcus, Aqueous sample introduction into a glow discharge device via a particle beam interface, Spectrochim. Acta B 46 (1991) 517.
[201] R. Pereiro, T.K. Starn, G.M. Hieftje, Gas-sampling glow discharge for optical emission spectrometry. Part II: Optimization and evaluation for the determination of nonmetals in gas phase samples, Appl. Spectrosc. 49 (1995) 616.
[202] R. Berneron, L'analyse des surfaces métalliques par spectrom étrie d' émission à décharge luminescente, Spectrochim. Acta 33B (1978) 665.
[203] D.G. Jones, R. Payling, S.A. Gower, E.M. Boge, Analysis of pigmented polymer coatings with radiofrequency glow discharge optical emission spectrometry, J. Analyt. Atom. Spectrom. 9 (1994) 369.

[204] A. Bengtson, Quantitative depth profile analysis by glow discharge, Spectrochim. Acta B 49 (1994) 411.
[205] Z. Weiss, Quantitative depth profile analysis by glow discharge optical emission spectrometry: an alternative approach, J. Analyt. Atom. Spectom. 10 (1995) 891.
[206] H. Hocquaux, Thin film analysis, in: R.K. Marcus (ed.), Glow Discharge Spectroscopies, Plenum Press, New York, 1993.
[207] J.A.C. Broekaert, Glow discharge atomic spectroscopy, Appl. Spectrosc. 49 (1995) 12A.
[208] B.J. Russell, A. Walsh, Resonance radiation from a hollow cathode, Spectrochim. Acta 15 (1959) 883.
[209] D.S. Gough, P. Hannaford, A. Walsh, The application of cathodic sputtering to the production of atomic vapours in atomic fluorescence spectroscopy, Spectrochim. Acta B 28 (1973) 197.
[210] A.E. Bernhard, Atomic absorption spectrometry using sputtering atomization of solid samples, Spectroscopy 2 (1987) 24.
[211] M. Parker, R.K. Marcus, Investigation of sample atomization using a power-modulated radiofrequency glow discharge source, Appl. Spectrosc. 50 (1996) 366.
[212] B.W. Smith, J.B. Womack, N. Omenetto, J.D. Winefordner, Approaching single atom detection with atomic fluorescence in a glow discharge atom reservoir, Appl. Spectrosc. 43 (1989) 873.
[213] W.O. Walden, W.W. Harrison, B.W. Smith, J.D. Winefordner, Multielement glow discharge atomic fluorescence using continuum sources, J. Analyt. Atom. Spectrom. 9 (1994) 1039.
[214] B.M. Patel, J.D. Winefordner, Laser-excited fluorescence of diatomic molecules of copper and lead in glow discharge sputtering, Appl. Spectrosc. 40 (1986) 667.
[215] M.R. Winchester, S.M. Hayes, R.K. Marcus, Determination of platinum and rhodium in γ-alumina catalysts by glow discharge atomization atomic absorption spectrophotometry, Spectrochim. Acta B 46 (1991) 615.
[216] S.A. Dashin, I.A. Mayorov, M.A. Bolshov, Direct analysis of solid samples by laser excited atomic fluorescence spectrometry with sample atomization by ion sputtering in a planar magnetron discharge, Spectrochim. Acta B 48 (1993) 531.
[217] C.L. Davis, B.W. Smith, M.A. Bolshov, J.D. Winefordner, Laser-excited atomic fluorescence of Eu, Y and Tm in a miniature glow discharge atom reservoir, Appl. Spectrosc. 49 (1995) 907.
[218] E.H. Piepmeier, Atomic absorption and fluorescence spectroscopies, in: R.K. Marcus (ed.), Glow Discharge Spectroscopies, Plenum Press, New York, 1993.
[219] K.R. Hess, W.W. Harrison, in: D.M. Lubman (ed.), Lasers and Mass Spectrometry, Oxford University Press, London, 1990, p. 205.
[220] Y. Iida, Laser vaporization of solid samples into a hollow cathode discharge for atomic emission spectrometry, Spectrochim. Acta B 45 (1990) 427.
[221] Z. Zhu, E.H. Piepmeier, Optogalvanic and optopotential signals in a glow discharge reveal electrode coupling effects, Spectrochim. Acta B 49 (1994) 1775.
[222] C.M. Barshick, R.W. Shaw, J.P. Young, J.M. Ramsey, Evaluation of the precision and accuracy of a uranium isotope analysis using glow discharge optogalvanic spectroscopy, Analyt. Chem. 67 (1995) 3814.
[223] K.R. Hess, Laser based methods, in: R.K. Marcus (ed.), Glow Discharge Spectroscopies, Plenum Press, New York, 1993.
[224] H. Falk, Einige theoretische Ueberlegungen zum Vergleich der physikalischer Grenzen thermischer und nich-thermischer spektroskopischer Strahlungsquellen, Spectrochim. Acta B 32 (1977) 437.
[225] P.G. Riby, J.M. Harnley, D.L. Styris, N.E. Ballou, Emission characteristics of chromium in hollow anode furnace atomization non-thermal excitation spectrometry, Spectrochim. Acta B 46 (1991) 203.
[226] D.C. Liang, M.W. Blades, An atmospheric pressure capacitively coupled plasma formed inside a graphite furnace as a source for atomic emission spectroscopy, Spectrochim. Acta B 44 (1989) 1059.
[227] R.E. Sturgeon, S.N. Willie, V.T. Luong, S.S. Berman, Characteristic temperatures in a FAPES source, Spectrochim. Acta B 46 (1991) 1021.
[228] J.M. Harnly, D.L. Styris, P.G. Rigby, Discharges with graphite furnace atomizers, in: R.K. Marcus (ed.), Glow Discharge Spectroscopies, Plenum Press, New York, 1993.
[229] G.S. Lomdahl, J.V. Sullivan, Use of a boosted-output lamp for analysis of powdered rocks and metals, Spectrochim. Acta B 39 (1984) 1395.
[230] N.P. Ferreira, J.A. Straus, H.G.C. Human, Developments in glow discharge emission spectrometry, Spectrochim. Acta B 38 (1983) 899.
[231] F. Leis, E.B.M. Steers, Boosted glow discharges for atomic spectroscopy—analytical and fundamental properties, Spectrochim. Acta B 49 (1994) 289.
[232] Z. Shi, S. Brewer, R. Sacks, Application of a magnetron glow discharge to direct solid sampling for mass spectrometry, Appl. Spectrosc. 49 (1995) 1232.
[233] C. Molle, M. Wautelet, J.P. Dauchot, M. Hecq, Characterization of a magnetron radiofrequency glow discharge with a glass cathode using experimental design and mass spectrometry, J. Analyt. Atom. Spectrom. 10 (1995) 1039.
[234] M.J. Heintz, G.M. Hieftje, Design and characterization of a planar magnetron radiofrequency glow discharge source for atomic emission spectrometry, Spectrochim. Acta B 50 (1995) 1109.
[235] A.R. Raghani, B.W. Smith, J.D. Winefordner, A miniature planar magnetron glow discharge source for analysis of submicroliter volume aqueous samples using atomic emission spectroscopy, Spectrochim. Acta B 51 (1996) 399.
[236] M.J. Heintz, J.A.C. Broekaert, G.M. Hieftje, Analytical characterization of a planar magnetron radiofrequency glow discharge source, Spectrochim. Acta B 52 (1997) 579.
[237] P.R. Banks, M.W. Blades, Atomic emission spectroscopy using a jet-assisted glow discharge source, Spectrochim. Acta B 44 (1989) 1117.
[238] J.A.C. Broekaert, T. Bricker, K.R. Brushwyler, G.M. Hieftje, Investigations of a jet-assisted glow discharge lamp for optical emission spectrometry, Spectrochim. Acta B 47 (1992) 131.

[239] H.J. Kim, Y.S. Park, J.H. Cho, G.H. Lee, K.H. Cho, K.B. Lee, H.S. Kim, Studies of jet configurations for jet-enhanced sputtering devices, J. Analyt. Atom. Spectrom. 10 (1995) 335.

[240] M.R. Winchester, M.L. Salit, Design and initial characterization of a glow discharge atomic emission instrument for macro-scale elemental composition mapping of solid surfaces, Spectrochim. Acta B 50 (1995) 1045.

[241] Y. Kanzaki, N. Nishimura, O. Matsumoto, On the yields of glow discharge electrolysis in various atmospheres, J. Electroanalyt. Chem. Interfacial Electrochem. 167 (1984) 297.

[242] T. Cserfalvi, P. Mezei, P. Apai, Emission studies on a glow discharge in atmospheric pressure air using water as a cathode, J. Phys. D 26 (1993) 2184.